The Jewish National Fund (JNF)

CREATING WATER SENSITIVE CITIES IN ISRAEL

Project 2.1: Water Sensitive Urban Planning and Design

Third annual progress report

Prof. Evyatar Erell, Dr. Aviva Peeters, Dr. Shai Kaplan and Dr. Bin Zhou

The Jacob Blaustein Institutes for Desert Research
Ben-Gurion University of the Negev

April 2018

1. Introduction

Project 2.1 comprises two sub-projects:

The first sub-project seeks to establish and demonstrate a methodology for obtaining a detailed spatial distribution of storm water in an existing urban location, and a tool for deciding how to allocate the resource to locations where the water may be treated, stored, recharged or used. The study takes into account the size, geometry and land use patterns of catchment areas in prototypical urban typologies of Israeli cities.

The second sub-project attempts to provide a quantitative assessment of specific benefits from extensive planting of vegetation supported by storm water harvesting and treatment in existing urban areas, with regard to pedestrian thermal comfort and conservation of energy in buildings. The study investigates by means of computer simulation the integrated effect of vegetation on air temperature, humidity, radiant exchange and wind speed – all of which affect both pedestrian comfort and building energy performance.

Work on both sub-projects proceeds in parallel. A proof-of-concept study will first demonstrate that the methodology can, in principle, estimate local-scale benefits to urban amenity from the implementation of generic WSUD elements, in the context of Israeli urban morphology and climate. As detailed, site-specific WSUD solutions are implemented in the proposed urban renovation plans, the climate and energy models will be updated to assess the effect of these actions.

An overview of the two component sub-projects of the research follows below.

1.1 Development of a methodology for identifying and mapping effective retrofit of physical infrastructure in existing urban areas to utilize storm water

To improve storm water runoff management and harvesting in existing urban areas, it is important to first recognize and map the existing urban typology, the spatial runoff network in the city and the sub-surface hydrology. A GIS-based spatial analysis provides the framework, methods and tools to apply a quantitative analysis which can take into account all the parameters that play an important role in defining the surface water drainage network. The ArcGIS software package (ESRI, 1984) includes hydrological modelling capabilities, which combined with the SUSTAIN hydrological model (Shoemaker, 2009; 2011; 2013) provide a set of powerful tools for characterizing surface runoff. Parameters such as land-use and land cover, proportion of impervious areas, soil type, meteorological data (precipitation and evapotranspiration), elevation and slope are used to delineate the surface flow direction and accumulation and eventually the flow path network. Input data on urban cover is obtained from the Israeli national mapping agency or from local city authorities. This part of the study will build upon current work being carried out within Australian CRC for Water Sensitive Cities (Project A4.3: Socio-technical modelling tools to examine urban water management scenarios, http://watersensitivecities.org.au).

Once the existing flow network and potential water accumulation is established, the infiltration/runoff ratio can be determined and locations for bio-filtration systems or modular systems can be defined. Such locations should consider the quality of filtrating water and be situated in a way to harvest higher quality runoff water at source and prevent it from mixing with runoff water of low quality such as runoff generated from industrial areas and roads. The calculated infiltration/runoff ratio will be used to derive the potential amount of water which will be diverted for above-ground runoff harvesting. Data received from project 1.2, such as hydrographs and pollutographs, will be used to refine and validate the GIS model. In addition, GIS-based spatial analysis will be used to superimpose layers of various parameters such as microclimate, vegetation, water quality and runoff accumulation to recognize spatial correlations among them.

The primary application of the model will be to make the most effective use of storm water near the source, preferably for aquifer recharging, while existing infrastructure for storm water conveyance (removal from the sites) will be used to manage overflow in case of intense rain events. A second aim of the project is to enhance the quality of life in cities. Because conditions in Israeli cities are different from those in, for example, Melbourne, the implementation of storm water facilities may need to be different, too. Since Israel has a prolonged completely dry season, water is not available to be used directly to produce cooling by evaporation when it is most needed; Moreover, since cities in Israel have less open space in which to plant vegetation, which is an integral feature of many SW facilities, achieving measurable effects on microclimate will require very careful integration in the urban fabric.

Of specific interest in this context is the selection of appropriate vegetation, which is not only compatible with storm water harvesting infrastructure but which will also contribute the most to increased quality of life. Research has demonstrated that in Israeli conditions, the most effective use of vegetation to improve pedestrian thermal comfort is to plant shade trees; the contribution of grass to comfort is relatively minor – yet requires much more water (Shashua-Bar *et al*., 2009; 2011).

The project will examine integration of tree planting in storm water treatment and bio-filtration facilities, building on the work of Galon and Heller (2010), who provided an authoritative guide to planting trees in city streets. Their study, carried out on behalf of the Ministry for Environmental Protection and the Ministry of Agriculture, focused on integrating trees in the design during the planning phase of new neighbourhoods, and covered such aspects as the recommended cross-section of streets, coordination with sub-surface infrastructure and the suitability of tree types to Israeli conditions.

The final outcome of the project will include case studies of two Israeli cities (near the coast and in an inland location; Bat-Yam and Ramla or/and Kfar Saba), which will test the methodology and demonstrate the applicability of retrofit interventions in the physical infrastructure at different scales. Such actions may include creation of micro-catchment areas diverting water to small modular treatment and recharge units (MFUs); collection of storm water from private open space or parking lots and diverting it to newly created planted areas; or diversion of storm water from streets to small neighbourhood parks or filtration and aquifer recharge units (such as the one in Kfar Saba).

1.2 Modelling the effect of vegetation supported by stormwater harvesting on the microclimate of existing urban areas

One of the benefits of water sensitive urban design is enhancement of quality of life, and in particular, modification of urban microclimate and mitigation of the urban heat island. However, the focus on studying the effects of vegetation on air temperature has been accompanied by insufficient attention to the complexity of the processes that affect the desired practical outcomes. For example, although a majority of the studies on the effects of vegetation focus on reduction of air temperature, typically in the context of mitigating the urban heat island, air temperature is only one of several factors that affect pedestrian thermal comfort in outdoor spaces; in warm, sunny climates such as Israel, radiant exchange is much more important (Shashua-Bar *et al*., 2009; 2011).

It is therefore suggested that the study of the effects of vegetation supported by storm water should be carried out by means of models that were implemented to answer practical questions that require detailed description of what is typically a very complex reality. In particular, useful conclusions may be drawn regarding the following issues:

a. How does adding vegetation affect the *energy consumption of buildings* in typical urban settings in Israel?
b. How does vegetation, especially trees, affect *pedestrian thermal comfort*?

Nice (2012) noted in a survey of computer modelling tools that evaluate the impacts of WSUD on human thermal comfort in urban areas that assessment required a number of different tools. The present study therefore employs a three-step computer modelling study to answer these questions.

The first step is the analysis of microclimate in representative locations of the cities where storm water harvesting pilot studies are proposed. The analysis is carried out using the CAT model (Erell & Williamson, 2006), which uses meteorological data from a representative (non-urban) weather station in the region to generate time series of local-scale meteorological parameters at an urban street canyon. The transformation is based on a complete surface energy balance at the two sites. In addition to a 2.5-dimensional analysis of radiant exchange accounting for short and long-wave fluxes, it incorporates several elements of the LUMPS parameterization scheme (Grimmond & Oke, 2002), including moisture advection from nearby vegetation and bodies of water, as detailed in Erell *et al*. (2010). The effect of turbulent mixing in different stability regimes is estimated by means of an empirical correlation validated using site data from Adelaide and Goteborg.

The CAT model currently describes vegetation using fairly coarse parameterizations linking surface cover with advection of moisture and latent heat. The proposed research will seek to provide a more detailed treatment. Model performance will be tested using field data from Adelaide (Erell & Williamson, 2007); Goteborg (Eliasson et al, 2006); and Melbourne (using monitoring data provided by Monash partners).

The outputs of the CAT model, including localized air temperature, wind speed, relative humidity and the temperatures of ground and wall surfaces, will then be used as inputs to two additional models:

a. The impacts of vegetation on pedestrian thermal comfort will be modelled using the Index of Thermal Stress (ITS). The ITS (Pearlmutter *et al*., 2007) is a measure of the rate at which the human body must give up moisture to the environment in order to maintain thermal equilibrium, in response to both metabolic heat production and to heat exchange with the environment. The value of the index (ITS) is the ratio between the sweat rate required for thermal equilibrium and a cooling efficiency which is estimated by an empirical relationship that accounts for the humidity of the air, wind speed and the insulation value of the clothing (assumed to be small). To calculate the value of the index, a full energy balance must be evaluated for the pedestrian (approximated by a cylinder) and the surroundings, accounting for net short wave radiation (direct, diffuse and reflected from adjacent surfaces, as well as reflected from the skin); long wave radiation (received from the sky and from terrestrial surfaces, and emitted by the skin); and convection with the surrounding air. The ITS in its present form describes the environment surrounding the pedestrian in terms of two walls and a ground surface. To account for vegetation, a further level of detail will be added to the model, to account for the compound effects of vegetation on the energy balance of a pedestrian, in addition to modifications of microclimate already accounted for by CAT.

b. The energy consumption of buildings may be predicted by computer simulation. The calculation requires a detailed description of the geometry and construction of the building, a schedule for operation of equipment to account for occupancy and internal loads and a description of local climate. Many building simulation software packages come with inbuilt climate data files, which include hourly data for a Typical Meteorological Year (TMY). TMY files are compiled from long term records at weather stations such as airports, which are assumed to be representative of the surrounding area. However, evidence of urban modification to weather indicates that the differences between city-centre locations and the typical rural reference sites used by meteorological services are often quite substantial. The CAT software may be used to generate a location-specific weather file. Appropriate descriptions of urban locations in the vicinity of storm water pilot projects, both in the initial condition and after the storm water treatment and vegetation are in place, will allow generation by CAT of two modified input files, for use by a building energy simulation tool such as EnergyPlus. Differences in the output of this last simulation will thus reflect the contribution of the added vegetation.

2. Progress update

2.1 Modelling ground surface temperature

The ground surface temperature is one of the most important controls on the urban microclimate: It affects both air temperature in the immediate proximity and the radiation balance with other objects and pedestrians in the street. The presence of moisture in the uppermost layer of soil (following rain events or irrigation) affects this temperature. Modelling the temperature should preferably be done by means of a simple and accessible tool, which would be available to consultants, and which would require a minimum number of inputs, publicly available from standard weather stations.

As outlined in the report for Year 2, such a model was assembled, based on elements drawn from several existing schemes which were modified to require only data that may be expected to be widely available. The model has been validated using meteorological data and surface temperature data from Sde Boqer, and performs very well in a variety of conditions. The model is now implemented in FORTRAN and has been integrated in the Canyon Air Temperature (CAT) model. A research paper describing the model and validation in detail was prepared and submitted for publication.

The revised paper, amended in response to reviewer comments, has now been accepted and published (Leaf and Erell, 2017). It is attached to this report as **Appendix 1**.

2.2 Modifications to the Canyon Air Temperature (CAT) model

Creating an interface between CAT and a GIS software was seen as an essential step in mapping the integrated effect of vegetation on urban microclimate simultaneously for a large number of locations in a real city. CAT was initially conceived as a computer program designed to generate urbanized descriptors of meteorological conditions, especially air temperature, drawing upon measured data from a standard weather station in the region (typically, but not necessarily, located at the airport). The simulation requires a description of the geometry of the urban street canyon and details of land use and land cover (LULC). CAT was originally drawn up to calculate conditions in one urban location only. The interface with GIS software allows us to carry out the CAT simulation automatically for a large number of points within the urban fabric.

An interface was first written to read the data from the GIS in a systematic manner, and then to generate the input files required by CAT for each of the urban sites. A second procedure was then written to organize CAT output in a format that allows dynamic visualization of the simulation products, describing the evolution of air temperature across the city at hourly time steps.

The interface was described in a journal paper, which was published in *Applied Geography* (Kaplan et al, 2016) and was appended to the second annual report. The procedure has now been further refined, as follows:

Albedo

Landsat 8 images are used to estimate albedo with an empirical formula previously developed for the Landsat TM/ETM+ sensor (Liang, 2001):

$$\alpha = 0.356*b2+0.13*b4+0.373*b5+0.085*b6+0.072*b7-0.0018,$$

where b2, b3, b4, b5, b6 and b7 correspond to the reflectance in Landsat-8 spectral bands 2 (0.45-0.515 µm), 3 (0.525-0. 60 µm), 4 (0.63-0.68 µm), 5 (0.845-0.885 µm), 6 (1.560-1.660 µm) and 7 (2.1-2.3 µm), respectively. The building footprints are then masked, and the mean albedo for each grid cell is calculated and incorporated into the CAT model.

Vegetation and water fraction

CAT entails a detailed description of vegetation and water fractions in each grid cell and its vicinity, which accounts for the advection of moisture from source areas that are defined by wind direction and stability (Erell et al, 2009; 2010). Vegetation fraction is estimated from Sentinel-2 images at 30 m resolution using an unsupervised maximum likelihood classifier. Initialized with 50 land use/land cover classes, the identified classes are later collapsed into 4 types: roads, built-up, desert and vegetation. In the city of Beer Sheva, no significant surface water body exists due to the semi-arid climate dominating the region.

The vicinity of each cell is partitioned into 32 wedges based on pre-assigned azimuths and distances: 16 pie-shaped slices of 22.5° per each are further divided into 2 concentric segments at distances of 100-500 m and 500-1000 m away from the grid cell center. The vegetation fraction of each wedge is calculated based on the gridded land use/land cover map generated above.

Street width

After scrutinizing the geospatial data on streets and building footprints provided by the municipality and the Israel Mapping Agency (MAPI), we modified our method to derive the average street width in response to deficiencies in existing data. As road pavements are not bound to lie in the center of urban street canyons, which are defined by the space between building facades on opposite sides of the street, the previous method relying on streets is prone to underestimate the street width. And even worse, in some cases line features for roads and building footprints intersect with each other, which results in erroneous estimation of street width. To overcome these shortcomings, we propose an enhanced method relying only on detailed inputs of building footprints.

Using the building footprint layer as input, a grid of 1x1 meter resolution raster cells is generated, which gives the distance from each raster cell to the closest building. The distance raster reaches its local maxima along the centerline between any two adjacent buildings. The set of local maxima constitutes the de facto urban streets. As the distance represents only half of the street, the real street width is double the local maxima. Taking into account the site-specific street characteristics, we introduced a minimum threshold of 20 m, i.e., only streets wider than 20 meters are regarded as streets in Beer Sheva. The street width of a grid cell is averaged over all streets within it.

Considering the fact that an urban street canyon (defined for the purpose of microclimatic analysis) can be formed even if there are no discernible paved roads between adjacent building blocks, our approach is capable of robustly describing urban geometry in a statistically sound way.

Street orientation

The street orientation (azimuth) is determined based on the de facto urban streets delineated above. We specified 0° for the north. Each link (edge) of streets in a grid cell is projected onto the cardinal directions. However, due to the symmetry of the street orientation, we restricted the orientation angle to 0-180°. The street orientation of a grid cell is the vector sum of street vectors within it.

Building height

For each grid cell, the mean building height is calculated by averaging heights of buildings within the very cell, weighted by their wall areas.

Anthropogenic heat

The urban surface energy balance (SEB) includes anthropogenic heat, primarily heat lost from buildings and from vehicle traffic. In early versions of CAT, this component of the SEB was derived from estimates obtained by a variety of methods, either top-down or bottom-up, in other cities. Values used were monthly city-wide averages, included in the CAT input files, which were then processed to generate a typical diurnal profile. This method was satisfactory for simulations in one urban site, provided an appropriate estimate of the urban average anthropogenic heat was available. The method is not capable, however, of describing intra-urban variations of heat emissions.

A methodology was therefore proposed to account for differences in emissions among neighbourhoods of different density, at hourly time steps. It uses building height to estimate heat losses by conduction through facades, using typical thermal properties of walls and windows. To simplify the calculation procedure, conduction is assumed to be proportional to the difference in air temperature between the building interior (25^{o}C in summer, 20^{o}C in winter) and exterior. Heat loss by convection is estimated assuming a fixed number of air changes per hour between the interior and the exterior, again based on the difference between internal and external air temperature. The building volume is estimated from its height and assuming a fixed depth (measured from the street façade) of 10 meters. The number of air changes per hour is fixed at 2, an estimate that is based on the construction quality and airtightness of fenestration in Israel. In summer, heat ejected by air conditioners is assumed to be proportional to the difference in air temperature between the interior and exterior. Heat emitted by automobiles is estimated as the product of the heat emitted by an average car – 3,795 J/m (Sailor & Lu, 2004) - and the number of vehicles travelling down the street. The latter number is very difficult to obtain, and requires detailed traffic counts or proxies generated by navigation apps such as Waze – which are not available to us at this point. A simplified procedure, which is necessarily crude, assigns automobile traffic to the street in a given location based on street width (broad streets have higher traffic) and time of day. The diurnal hourly profile accounts for a minimum load at night, maximum load during the morning and afternoon peak hours, and intermediate loads at other times.

2.3 Validation of the revised CAT model

Validation of the new version of the CAT model was performed by comparing measurements made in the Israel Meteorological Service weather station in central Beer Sheva (N31.251 E34.799) with simulated values generated by CAT for the same location using data from the Nevatim station, about 12.8km to the southeast (N31.2050 E34.9227). This allows us to assess the ability of CAT to simulate the urban effect, which is the outcome of the interaction among several factors, including land cover, building geometry, vegetation and anthropogenic heat.

Figure 1 shows a time series for a period of 7 days at the end of July 2016. The urban effect on air temperature is quite weak during daytime, and may in fact be exhibited in a very small reduction in peak air temperature at mid-day, and a still-modest heat island at night. The night-time heat island is primarily due to restricted long wave radiant cooling. The contribution of anthropogenic heating at night during summer is minimal, because vehicle traffic is very small and there is very little heat emission from buildings, either through the envelope (conduction or convection) or by air conditioning plant. Daytime anthropogenic heating is higher due to vehicular traffic, but Beer Sheva is relatively dispersed and the weather station, which is located in an open area at the old campus of the Negev Research Institute (near City Hall) exhibits few urban characteristics.

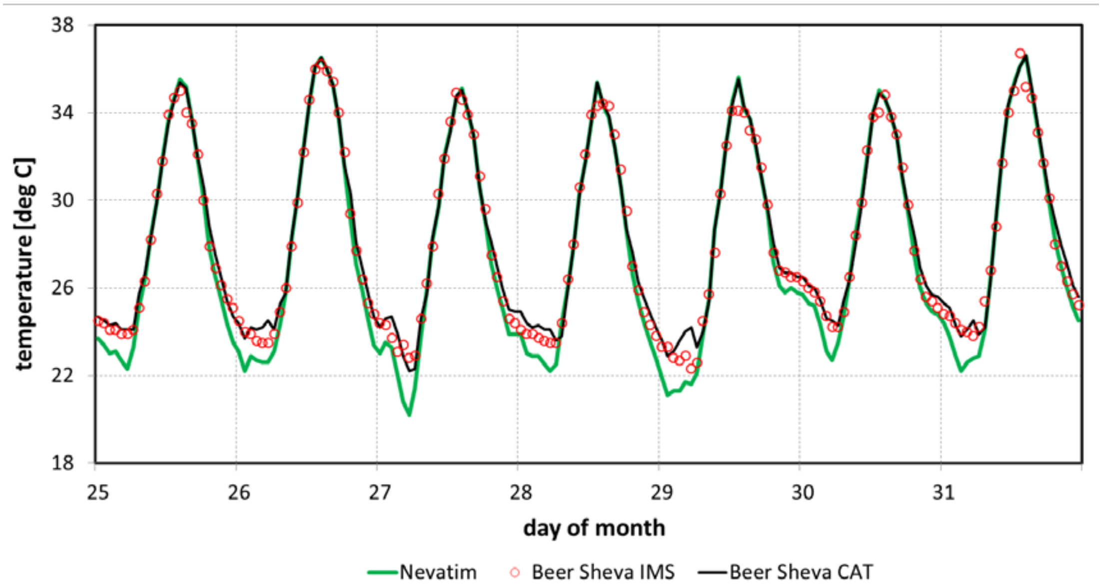

Figure 1.

Time series showing air temperature measured at Beer Sheva and Nevatim, and simulated values generated by CAT for the last week of July 2016.

The scatter plot showing measured and modelled air temperature for Beer Sheva during the month of July 2016 (Figure 2) confirms the visual impression given in the time series plot. Likewise, the summary of goodness-of-fit statistics (Table 1) is an indication of the overall robustness of the modelling methodology.

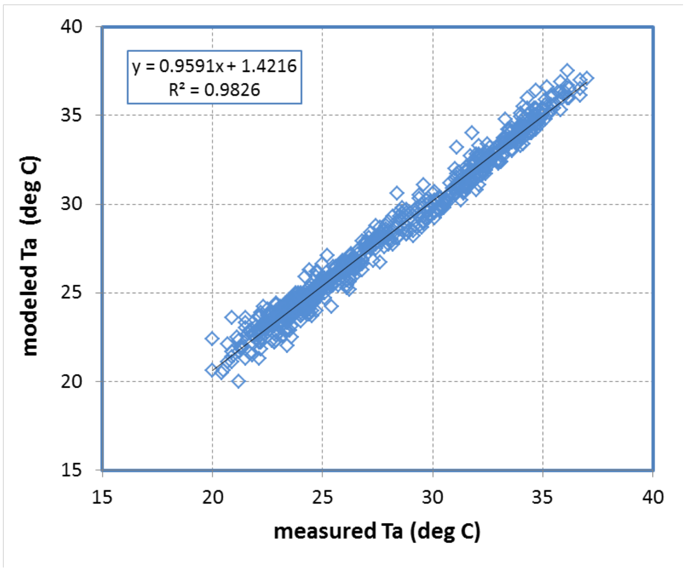

Figure 2.

Scatter plot showing measured and modelled air temperature for Beer Sheva during the month of July 2016. CAT model output is derived from measured data outside the city.

Table 1. Error statistics for the CAT model of Beer Sheva air temperature for the month of July 2016.

N	744	hours
Mean error	-0.29	^oC
Minimum error	-2.67	^oC
Maximum error	1.37	^oC
Std Deviation	0.58	^oC
MSE	0.42	^oC
Systematic MSE	0.11	^oC
Unsystematic MSE	0.31	^oC
Willmott index	0.99	
Degree of confirmation*	0.24	

* According to the Williamson degree of confirmation (Williamson, 1995), a model will be considered effective if the predicted value (in this case modelled air temperature) will provide a better fit to the measured value than an arbitrary estimate such as the input value (in this case measured air temperature at Nevatim). The indicator varies from $-\infty$ to 1.0, with values between 0.0-1.0 indicating an improvement relative to the arbitrary reference.

2.4 Simulation of spatial variations of urban air temperature using CAT

To demonstrate the ability of the CAT model to analyse the air temperature variations for an entire city using the new model, a simulation was carried out for the city of Beer Sheva. The city and its vicinity were divided into a total of 10,400 grid cells at a size of 90x90 m^2.

Analysis of the surface and land cover characteristics of Beer Sheva, which were incorporated in the input for the CAT simulations, is presented in Figure 3.

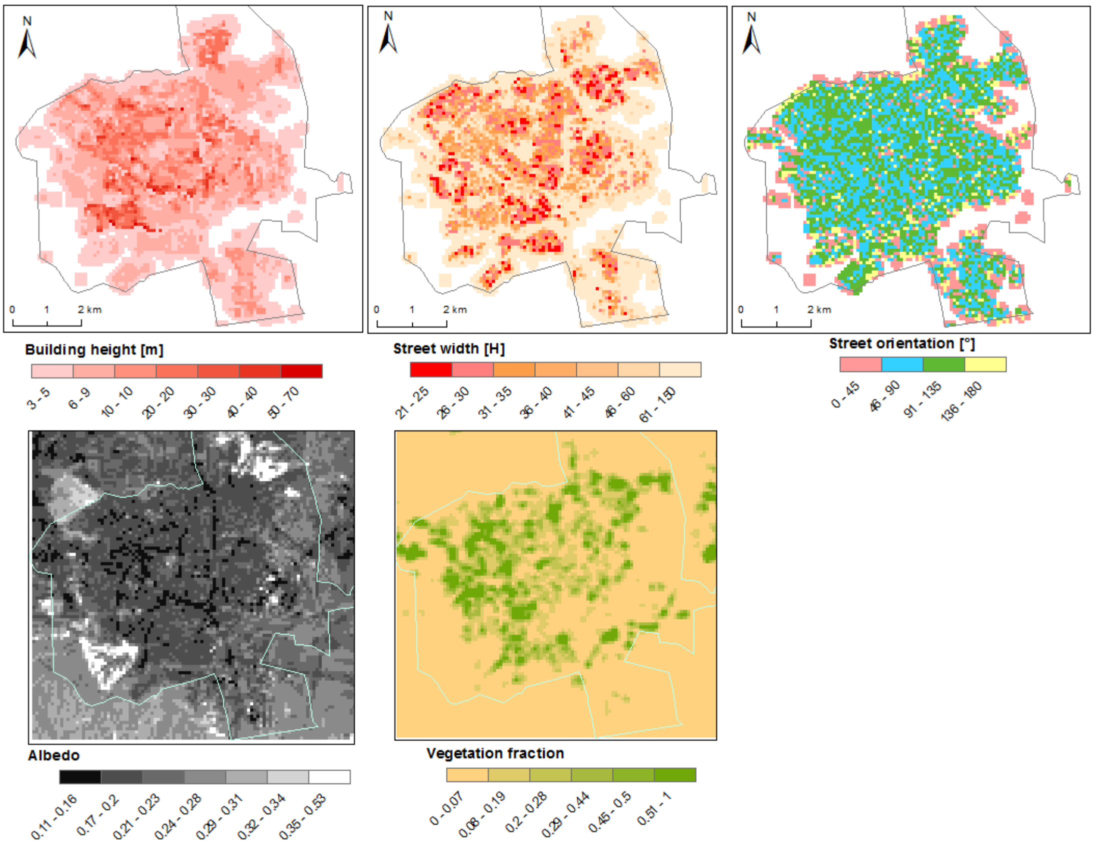

Figure 3.

The spatial distribution of land use and land cover in Beer Sheva. The underlying data are incorporated in input for each pixel simulated by CAT.

The spatial distribution of intra-urban differences in air temperature in Beer Sheva, simulated by CAT for a 24-hour period on July 26-27, 2016, is shown in Figure 4. The reference temperature in each case is the temperature measured at the Nevatim weather station at the same time. As demonstrated in numerous studies all over the world, the urban heat island (UHI) is primarily a nocturnal phenomenon. It begins to form shortly after sunset, is clearly visible at 22:00 (top left panel) and reaches a maximum value later at night. In the case of Beer Sheva, the intensity of the UHI in summer is fairly modest, reaching a maximum of about 3 degrees (top right panel). This is because Beer Sheva is relatively dispersed, with mostly low and mid-rise buildings and broad streets. By early morning, the UHI has mostly dissipated, and temperature in the city is similar to the temperature recorded at Nevatim (bottom left panel). Intra-urban temperature differences remain small throughout the day (bottom right panel).

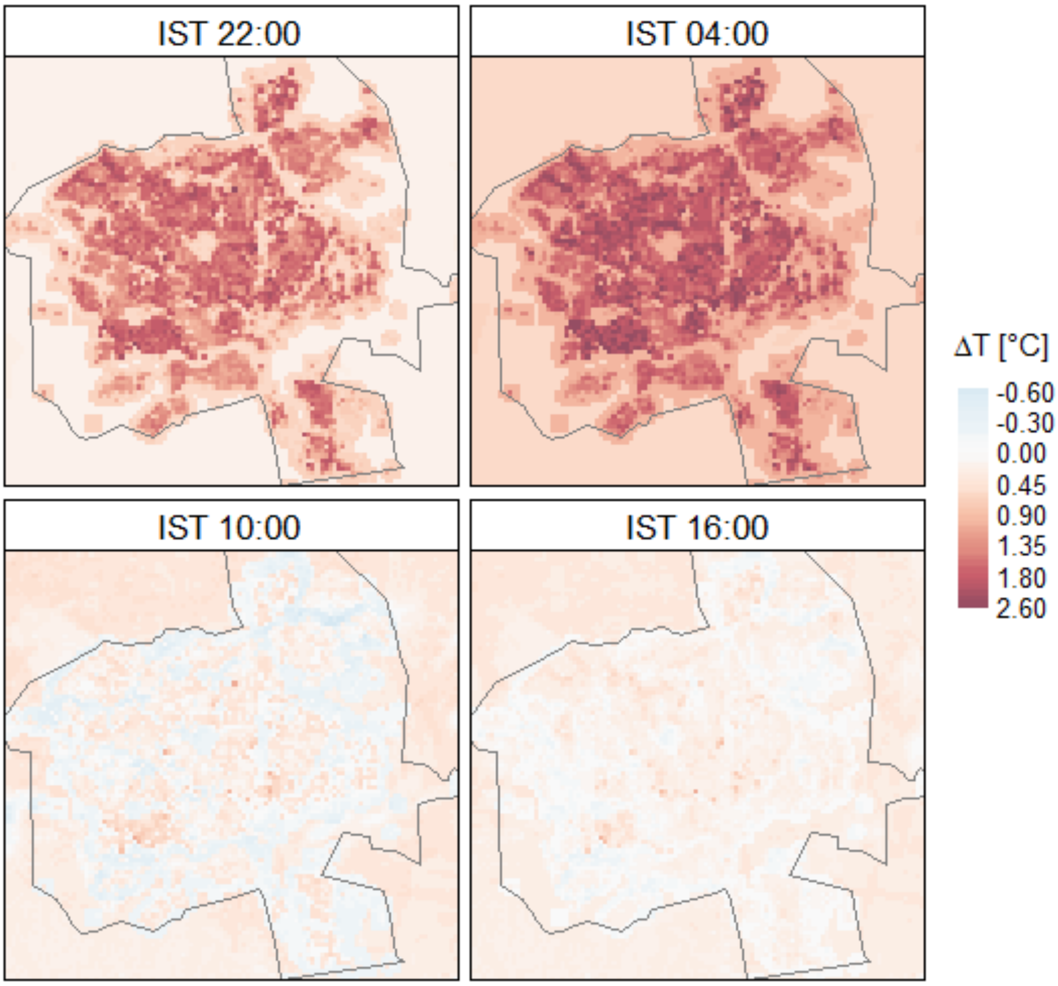

Figure 4.

The spatial distribution of intra-urban differences in air temperature in Beer Sheva simulated by CAT for a 24-hour period on July 26-27, 2016 (IST=Israel Standard Time). Temperature differences are displayed relative to the air temperature measured at the Nevatim weather station. The continuous black line represents the municipal boundary of the city.

It is of some interest to compare the simulated air temperature with Land Surface Temperature obtained by satellite (Figure 5). During daytime, the bare desert loess soil around the city, which is dry and has less thermal mass than urban surfaces, warms up more quickly, so that the city appears as an urban cool island (left pane). The coolest pixels in the image (surrounded by a rectangular frame on the left side of the image) are the irrigated fields of Kibbutz Hatzerim. The warm patch neat the center of the city (indicated by the circle) is the old Moslem cemetery, which has no vegetation and no buildings, and in many ways resembles the exposed rural soil. At night, the situation is reversed (pane on right): The rural surface cools down more quickly, so that the nocturnal urban heat island becomes readily apparent. The fields of Kibbutz Hatzerim are still distinguishable (see area surrounded by rectangle), and the urban surface is almost uniformly warmer.

The night time thermal image bears a strong resemblance to the simulated air temperature (Figure 4 above). Daytime surface temperature anomalies are not reflected in the spatial pattern of air temperature, due to both horizontal mixing by advection and vertical mixing of the unstable atmosphere.

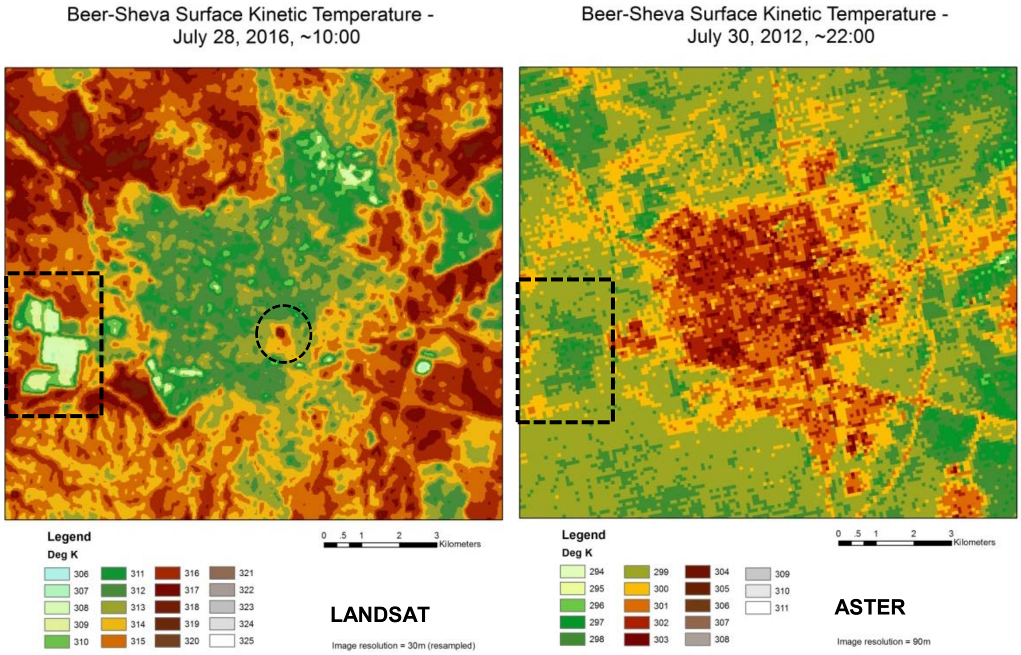

Figure 5.

The Land Surface Temperature of Beer Sheva during the daytime (left panel) and at night (right panel), on clear summer days.

2.5 Effect of vegetation in the bio-filters on pedestrian thermal comfort

One of the advantages of BMPs that include vegetation, in general, and of bio-filters in particular, is that they contribute to the thermal comfort of pedestrians. We have been asked to assess the potential benefit of several different types of plants considered for use in bio-filters. The plants being considered are illustrated in Table 2:

Table 2.

Plants being considered for use in bio-filters in Israel. Key: Blue outline – grasses; red outline: bushes or small trees; pink outline: small flowering plants. (Plants marked with a red X have now been discarded from use).

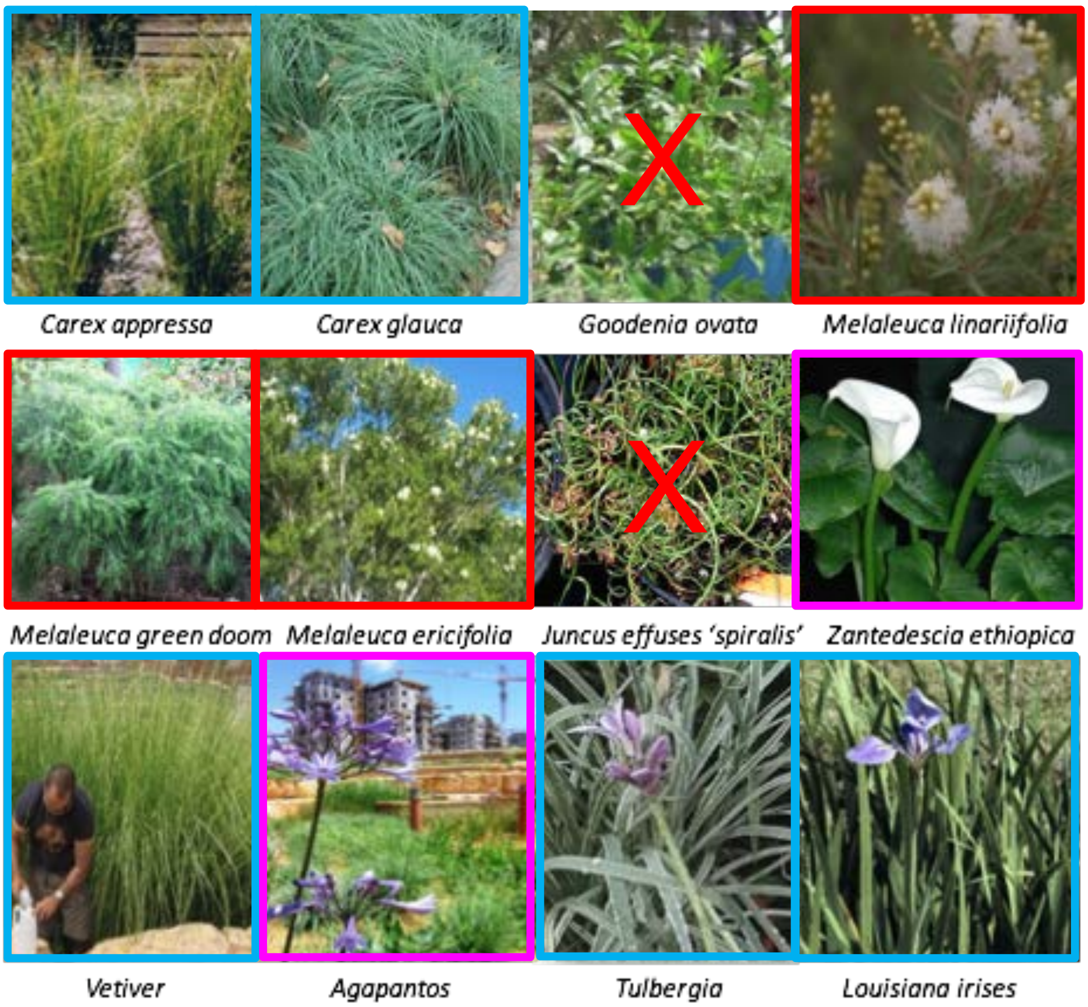

None of the plants in the table above appear on a list of water-conserving plants recommended by the Israel Ministry of Agriculture for use in landscaping (Israel Ministry of Agriculture, 2008). However, similar plants that are available in Israel and are generally considered water-conserving might be suitable for incorporation in the bio-filters. They should be investigated in future experiments with the bio-filter as possible replacements for the existing plants.

These generally fall into two categories: Large bushes, mostly variants of *Melaleuca*; and grasses, mostly variants of *Carex*.

Most melaleucas are endemic to Australia, but they may be found in a wide variety of habitats. The genus comprises close to 300 species, which have different characteristics. The species pictured below (Figure 6) - *Melaleuca lanceolate, Melaleuca elliptica* and *Melaleuca bracteata* - are found in Israel and are generally suitable for planting in a variety of soils and in different climate regions (http://www.tokeep.co.il/). They are hardy and require little maintenance and only modest irrigation.

Figure 6.

Three species of Melaleuca found in Israel. (http://www.tokeep.co.il/)

Carex is a vast genus of more than 2,000 species, also known as sedges, which may be found across most of the world. Most (but not all) sedges are found in wetlands, so their suitability to the bio-filters depends on a generous supply of water, although some species are fairly tolerant to drought. The species pictured below (Figure 7) - *Carex flava, Carex morrowii 'Variegata'* and *Carex testacea* - are found in Israel and are may be suitable, but there is probably no species that will thrive all over the country (http://www.tokeep.co.il/).

Figure 7.

Three species of Carex found in Israel. (http://www.tokeep.co.il/)

Small flowering plants, including the ones incorporated in the bio-filters, typically require substantial irrigation, and although their aesthetic contribution is undeniable, their contribution to thermal comfort is very modest.

To assess the possible contribution of the different plants used in conjunction with the bio-filters, their effects on microclimate must be understood. These will be discussed in brief in the next paragraphs. However, it should be recognized that the effect most commonly attributed to them, lowering ambient air temperature, is highly unlikely to be a major contribution of bio-filters because of their compact overall area. This does not mean, however, that they have no microclimatic benefits.

Uniquely among urban surfaces, plants have both a very low albedo, typically about 0.20-0.25 (meaning that they reflect very little sunlight), and a low surface temperature, so they emit less long wave radiation than other surfaces. This is possible because plants remain cool by evapotranspiration, which occurs when stomata are open during photosynthesis. However, evapotranspiration requires a sufficient supply of water – a limitation on employing large planted areas in landscaping in dry regions.

In contrast to surface cover plants, whose main contribution to human thermal comfort is through mediation of radiant energy transfer at the surface, trees in addition provide shade, mitigating the effect of direct solar radiation on pedestrians as well as reducing the solar flux on the ground surface.

A series of studies carried out in Sde Boqer (Shashua-Bar et al 2009, 2011; Snir et al, 2016) demonstrated the relative contribution of trees, grass and other surface cover plants to pedestrian thermal comfort. The contribution to thermal comfort was analysed in terms of the reduction to thermal stress, as indicated by the Index of Thermal Stress (Givoni, 1963; Pearlmutter et al, 2007). A ‘cooling efficiency’ was defined as the ratio between the reduction thermal stress and the latent heat of vaporization of the water lost by the plants (both expressed in W/m^2). The results of these studies may be summarized as follows:

1. Vegetation may make a substantial contribution to thermal comfort even when its effect on air temperature is negligible.
2. A planted surface can substantially reduce the energy load on a pedestrian
    - because of lower surface temperature (so there is less IR radiation)
    - because of lower albedo (so there is less reflected sunlight)
3. Various landscape treatments have demonstrated a clear contribution to pedestrian comfort, with the greatest reduction in mid-day thermal stress provided by a combination of shade trees and grass.

4. The vegetative treatment achieving the highest cooling efficiency in terms of water usage was shade trees alone.
5. Succulents are less effective than grass in lowering the surface temperature, but have a higher cooling efficiency than grass because of their lower water requirement.

The effect of surface cover plants on pedestrian thermal comfort can now be evaluated for a generic situation by means of computer simulation that combines the CAT model, which provides localized meteorological conditions in a given urban environment, including surface temperatures, and the Index of Thermal Stress, which is evaluated based on data generated by CAT. This procedure was demonstrated by Leaf and Erell (2017).

2.6 Application of methodology for selecting best management practices (BMP's) for management of urban runoff

In order to identify the most cost-effective BMPs for meeting water quality (pollutant reduction) and water quantity (flow mitigation) targets to manage urban runoff, the selected hydrological model should be able to:

- Model water quantity and water quality
- Model both surface and sub-surface networks
- Include a cost-benefit optimization module
- Operate on the scale of individual buildings

The SUSTAIN model (Shoemaker, 2009; 2011; 2013; Baek et al., 2015) which was selected as the preferred model for simulating runoff and BMP's (see annual report for Year 2) meets these objectives and is a free and open-source model. It was applied to the case study of Kfar Saba and was applied in a preliminary examination of the city of Bat-Yam. In addition to modelling optimal locations for a variety of BMPs, the runoff network was simulated in order to examine correlations between surface runoff and areas that were recognized by the model as suitable for BMP locations (Boulos *et al*., 2015; Sun *et al*., 2016).

It is important to note at this stage that an accurate urban database of high spatial-resolution is essential to draw substantial conclusions from locations suggested by the model for placing BMP's. The database must include street and sidewalk elevations as well as the elevation of other urban surfaces because analysis of the surface hydrological network is based on it. For example, in the case study of Kfar Saba an up-to-date and accurate DEM, received from the Kfar Saba municipality, ensured the integrity of surface runoff analysis and outputs. Consequently, the results coincide with the street network and the drainage system (Figure 8). The output of the hydrological analysis also includes a flow accumulation computation (the number of pixels contributing flow into each adjacent pixel). The measured precipitation allows calculation of the amount of surface runoff generated, supporting predictions of whether enough runoff will be accumulated at the locations suggested by the model for BMP siting.

In the case of Bat-Yam, only a basic DEM was accessible with a spatial resolution of 5 meters, which is insufficient for capturing differences in elevation of urban surfaces. The hydrological analysis resulted in a hydrological surface network which does not necessarily coincide with the actual urban land cover (Figure 9). Comparing BMP siting outputs for placing infiltration basins in Kfar-Saba (Figure 10) and Bat-Yam (Figure 11) highlights the difference in quality that is the result of insufficiently detailed inputs.

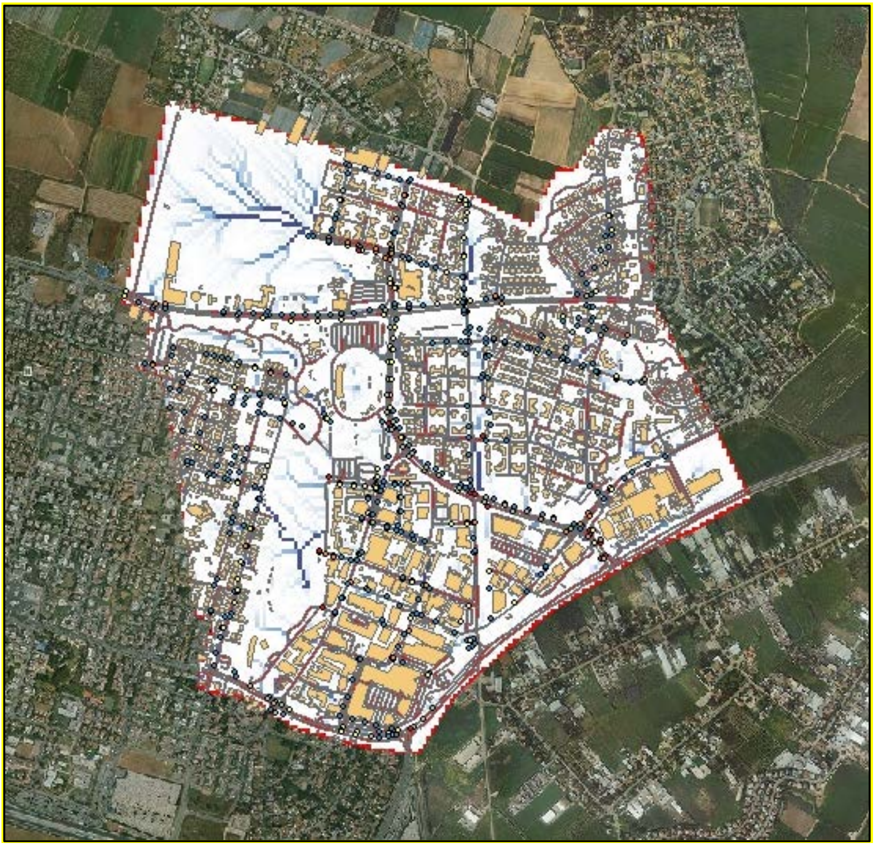

Figure 8.

Case study area in Kfar Saba showing the surface runoff hydrological analysis and its correlation with existing land-cover and drainage system

Figure 9.
Case study area in Bat-Yam showing the surface runoff hydrological analysis. In cases where only a basic DEM is available, without actual urban topography, the output does not necessarily correlate with the urban land-cover. See for example the area in the blue circle where modelled water paths appear to cross built-up land-cover.

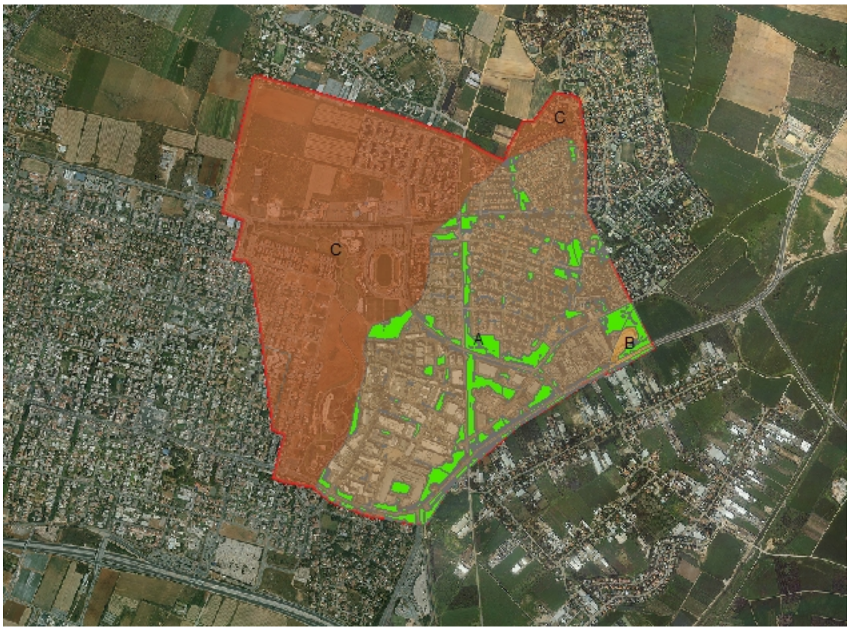

Figure 10.
BMP siting output for locating infiltration basins in the modeled catchment in the city of Kfar Saba. Note the influence of soil type on the location of infiltration basins which are not placed where the soil type has a tendency for erosion and development of gullies.

Figure 11.
BMP siting output for locating infiltration basins for an area in the city of Bat-Yam (note location of existing bio-filter).

An important attribute of the SUSTAIN model is the option to parameterize and customize a variety of attributes to comply with specific environmental and urban conditions. In addition, the parameters for placing each BMP such as slope, soil type, water table level, distance from buildings etc. can be manipulated to suit specific requirements (Figure 12). Each defined BMP can also be customized in terms of its structural details, dimensions, infiltration and cost factors. Site-specific solutions such as biofilters can thus be recommended, accounting for their total evaluated cost per unit.

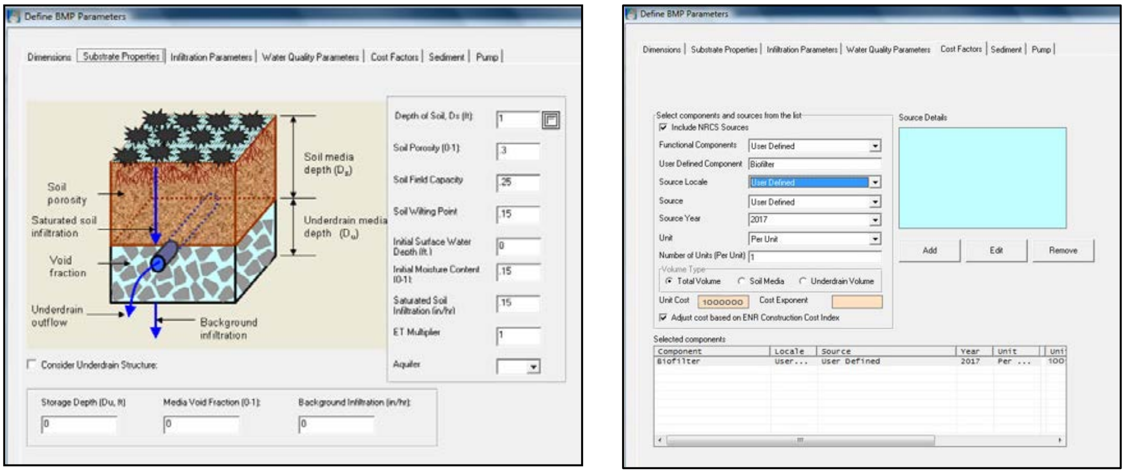

Figure 12.

Defining specific parameters to customize the BMP in terms of its substrate properties (left) and customizing the cost to define a per-unit overall cost such as for a biofilter (right).

Regrettably, the EPA has recently decided to stop supporting the SUSTAIN model for newer versions of Windows and ArcGIS (ESRI, 1984). It has been superseded by InfoSWMM (http://www.innovyze.com/products/infoswmm/), a commercial model which integrates the SWMM model and includes a BMP module and cost-optimization called InfoSWMM-Sustain, based on EPA's Sustain model. The model meets all objectives and is fully integrated within a GIS framework which streamlines the work process. Unfortunately, a fully functional version of the new software costs about $30,000, and requires a license that must be renewed annually at additional cost.

A limited free trial version of InfoSWMM, developed for student use, was downloaded and used to test runoff modeling in the Kfar Saba catchment. Similar to SUSTAIN it allows customization for specific environmental and urban conditions. For example, evaporation data can be input for each month as well as using a specific climatological file for temperature data or inputting monthly average wind speed. The study area can be subdivided into any number of irregular sub-catchments to represent the effect of spatial variability in terms of topography, land cover and soil. Low impact development (LID's) can be modeled in the simulation as well. This model will be further tested to examine its suitability.

In addition, other models were re-examined to determine which of them (if any) might be able to support abilities similar to the SUSTAIN model, and which will also meet the objectives stated at the beginning of this report. The only public-domain model which offers similar abilities to SUSTAIN and is also scientifically-grounded and widely-used is the SWMM model. However, it does not include a cost-optimization module; it is a stand-alone model (no GIS framework), its interface is not user-friendly and applying it requires a steep learning curve.

The Australian model MUSIC (https://ewater.org.au/products/music/) was examined as well. However, it is a lumped type model (Salvadore et al., 2015): such models are in general simpler than other models and may be most suitable when data are limited. MUSIC, for example, uses default values based on calibration of the model to typical urban catchments. Calibration for Israeli cities requires multiple storm water monitoring campaigns of several years duration – an exercise that is both costly and very demanding from a logistical perspective.

3. Work plan for Year 4

During Year 4, work will continue in parallel on both the hydrological modeling and further development and validation of CAT. The following objectives will be addressed:

- Refining the Kfar Saba model using InfoSWMM and applying the hydrological analysis to the Bat-Yam case study.
- Calibration of the model using data collected by the work group of Prof. Rony Wallach.
- Compiling a set of recommendations for selecting a suitable hydrological model.
- Report on effect of vegetation on building energy consumption – integrated modelling CAT and building energy software (e.g. Energy+)
- Integrated assessment of the effect of adding vegetation to modify urban microclimate in Israeli cities
- Conducting a workshop for introducing the concept of urban hydrological modelling in general and BMP siting in particular. The workshop will demonstrate the theory and application of BMP siting to a case study and will be accompanied by a tutorial for the use of drainage consultants, planners, decision makers and urban hydrologists.
- Final report with integrated methodology, application examples and design guidelines

4. References

1. Baek, S., Choi, D., Jung, J., Yoon, K. (2015), Evaluation of a hydrology and run-off BMP model in SUSTAIN on a commercial area and a public park in South Korea, *Desalination and Water Treatment*, 55(2):347-359.

2. Boulos, P. F., Barnett, T. C., Dickinson, R. E. (2015), Smart network modeling for effective planning of sustainable urban areas, *Journal of the American Water Works Association* 107(12): 54-58.

3. Eliasson, I., Offerle, B., Grimmond, C.S.B. and Lindqvist, S. (2006). Wind fields and turbulence statistics in an urban street canyon. Atmospheric Environment, 40:1-16.

4. Erell E. and Williamson T. (2006). Simulating air temperature in an urban street canyon in all weather conditions using measured data from a reference meteorological station. International Journal of Climatology 26:1671–1694.

5. Erell E. and Williamson T. (2007) Intra-urban differences in canopy layer air temperature at a mid-latitude city. International Journal of Climatology, 27:1243-1255.

6. Erell E., Eliasson E., Grimmond S., Offerle B. and Williamson T. (2009) Incorporating spatial and temporal variations of advected moisture in the canyon air temperature (CAT) model. ICUC7 - The 7th International Conference on Urban Climate, Yokohama, Japan, July 3-6 2009.

7. Erell E., Eliasson E., Grimmond S., Offerle B. and Williamson T. (2010). The effect of stability on estimated variations of advected moisture in the Canyon Air Temperature (CAT) model. The 9th AMS Symposium on the Urban Environment, Keystone, Co., Aug. 2-6 2010.

8. ESRI. (1984). ArcGIS® Desktop 10.0, copyright © 1999-2010 ESRI inc. Redlands, CA: Environmental Systems Research Institute, Inc. (ESRI).

9. Galon, I. and Heller A. (2010). Guide to Street Trees. Israel Ministry of Agriculture and Rural Development and the Israel Ministry for Environmental Protection. Electronic document, 112p (in Hebrew).

10. Givoni B. (1963). Estimation of the effect of climate on man: development of a new thermal index. PhD Thesis, School of Medicine, The Hebrew University, Jerusalem.

11. Grimmond, S. and Oke, T. 2002. Turbulent heat fluxes in urban areas: Observations and a Local-scale Urban Meteorological Parameterization Scheme (LUMPS). *Journal of Applied Meteorology* 41: p. 792-810.

12. Israel Ministry of Agriculture (2008). List of Water Conserving Plants (in Hebrew). http://www.moag.gov.il/subject/zmahim_jishoney_maim_2008/documents/reshimat_500_zmachim_chaschanim_bemaym.pdf

13. Kaplan S., Peeters A. and Erell E. (2016). Predicting air temperature simultaneously for multiple locations in an urban environment: a bottom up approach. *Applied Geography*, 76:62-74.

14. Leaf S. and Erell E. (2017). "A model of the ground surface temperature for micrometeorological analysis". *Theoretical and Applied Climatology*, in press. http://link.springer.com/article/10.1007/s00704-017-2207-5

15. Nice, K., Beringer J., Coutts, A. and Tapper N. (2012). Urban Climate Model Selection for Modelling WSUD Features. Report on Project 3: Green Cities and Micro-Climate, Centre for Water Sensitive Cities, 25p.

16. Pearlmutter D., Shaviv E. and Berliner P. (2007). Integrated modeling of pedestrian energy exchange and thermal comfort in urban street canyons. *Building & Environment*, 42:2396-2409.

17. Salvadore, E., Bronders, J., Batelaan, O. (2015), Hydrological modeling of urbanized catchments: A review and future directions, *Journal of Hydrology* 529: 62-81.

18. Sailor D. and Lu L. (2004). A top–down methodology for developing diurnal and seasonal anthropogenic heating profiles for urban areas. Atmospheric Environment 38:2737-2748.

19. Schiller, G. and Karschon, R. (1974). "Microclimate and recreational value of tree plantings in deserts", Landscape Planning 1: 329-337.

20. Shashua-Bar L., Pearlmutter D. and Erell E. (2009). "The cooling efficiency of urban landscape strategies in a hot dry climate". Landscape and Urban Planning, 92(3-4):179-186.

21. Shashua-Bar L., Pearlmutter D. and Erell E. (2011). "The influence of trees and grass on outdoor thermal comfort in a hot-arid environment". International Journal of Climatology, 31(10): 1498–1506.

22. Shoemaker, L. (2009), SUSTAIN – A Framework for Placement of Best Management Practices in Urban Watersheds to Protect Water Quality. U.S. Environmental Protection Agency, Washington, DC, EPA/600/R-09/095.

23. Shoemaker, L., Riverson Jr, J., Khalid, A., Zhen, J. X., Murphy, R. (2011), Report on enhanced framework (SUSTAIN) and field applications for placement of BMPs in urban watersheds, Report. U.S. Environmental Protection Agency, Washington, DC, EPA/600/R-11/144.

24. Shoemaker, L., Riverson Jr, J., Khalid, A., Zhen, J. X., Murphy, R., Wood, B. (2013), Stormwater Management for TMDLs in an Arid Climate: A Case Study Application of SUSTAIN in Albuquerque, New Mexico, Report. U.S. Environmental Protection Agency, Washington, DC, EPA/600/R-13/004.

25. Snir K., Pearlmutter D. and Erell E. (2016). "The moderating effect of water-efficient ground cover vegetation on pedestrian thermal stress". Landscape and Urban Planning 152: 1-12.

26. Sun, Y., Tong, S., Yang, Y. J. (2016), Modeling the cost-effectiveness of stormwater best management practices in an urban watershed in Las Vegas Valley, *Applied Geography* 76: 49-61.

27. Williamson T.J. (1995). A confirmation technique for thermal performance simulation models. Building Simulation '95, August 14-16, 1995, Madison, Wisconsin, U.S.A.

28. Willmott C.J. (1981). On the validation of models. Physical Geography 2:184–194.

APPENDIX 1

Leaf J. and Erell E. (2016). A model of the ground surface temperature for microclimate analysis. *Theoretical and Applied Climatology*, in press.

http://link.springer.com/article/10.1007/s00704-017-2207-5.

Theor Appl Climatol
DOI 10.1007/s00704-017-2207-5

ORIGINAL PAPER

A model of the ground surface temperature for micrometeorological analysis

Julian S. Leaf[1] **· Evyatar Erell**[1]

Received: 7 May 2017 / Accepted: 18 June 2017

Abstract Micrometeorological models at various scales require ground surface temperature, which may not always be measured in sufficient spatial or temporal detail. There is thus a need for a model that can calculate the surface temperature using only widely available weather data, thermal properties of the ground, and surface properties. The vegetated/permeable surface energy balance (VP-SEB) model introduced here requires no a priori knowledge of soil temperature or moisture at any depth. It combines a two-layer characterization of the soil column following the heat conservation law with a sinusoidal function to estimate deep soil temperature, and a simplified procedure for calculating moisture content. A physically based solution is used for each of the energy balance components allowing VP-SEB to be highly portable. VP-SEB was tested using field data measuring bare loess desert soil in dry weather and following rain events. Modeled hourly surface temperature correlated well with the measured data (r^2 = 0.95 for a whole year), with a root-mean-square error of 2.77 K. The model was used to generate input for a pedestrian thermal comfort study using the Index of Thermal Stress (ITS). The simulation shows that the thermal stress on a pedestrian standing in the sun on a fully paved surface, which may be over 500 W on a warm summer day, may be as much as 100 W lower on a grass surface exposed to the same meteorological conditions.

Electronic supplementary material The online version of this article (doi:10.1007/s00704-017-2207-5) contains supplementary material, which is available to authorized users.

✉ Evyatar Erell
erell@bgu.ac.il

1 The Jacob Blaustein Institutes for Desert Research, Ben-Gurion University of the Negev, 8499000 Sde Boqer Campus, Israel

Keywords Storage flux · Soil moisture · Evapotranspiration · Sol-air temperature · Sub-surface ground temperature

1 Introduction – modeling surface temperature

The temperature of different urban surfaces, whether impermeable concrete, permeable bare soil or vegetation, has an effect on urban micrometeorological conditions and urban climate (Mueller and Day 2005; Yilmaz et al. 2008), on pedestrian thermal comfort (Shashua-Bar et al. 2009, 2011; Lee et al. 2016), and on energy in buildings (Meier 1990-91). Surface temperature governs two important processes: sensible heat flux and longwave radiation emitted by the surface.

Modeling schemes for urban micrometeorological conditions may incorporate any of several methods for estimating surface temperature (T_s). If most street canyon surfaces are shaded, either by buildings or vegetation, it is convenient to assign a uniform fixed surface temperature to enable the estimation of emitted longwave radiation (Krayenhoff et al. 2014). Alternatively, the temperature of shaded surfaces may be set as being equal to air temperature (T_a), while the temperature on surfaces exposed to the sun is estimated based on a linear relationship between maximum solar elevation and maximum difference between T_a and T_s during clear day conditions (Lindberg et al. 2008). The surface temperature may also be approximated by the *sol-air temperature*, $T_{sol\text{-}air}$ (Mackey and Wright 1943), which is defined as "the equivalent outdoor temperature which will cause the same rate of heat flow at the surface and the same temperature distribution throughout the material as results from the outdoor air temperature and the net radiation exchange between the surface and its environment." In Eq. (1), T_a is the measured air temperature, $K_\downarrow$ is the incoming shortwave radiation, α is the albedo of the surface, ε is its emissivity, $L_\downarrow$ is the incoming

Published online: 13 July 2017

longwave radiation, $L_\uparrow$ is the longwave radiation emitted from the surface, and h_c is the convective heat transfer coefficient.

$$T_{\text{sol-air}} = T_a + \frac{(1-\alpha)\,K_\downarrow - \varepsilon\left(L_\downarrow - L_\uparrow\right)}{h_c} \tag{1}$$

This equation is relatively simple, and although it requires an iterative numerical solution to determine the emitted longwave radiation, it is incorporated in the Canyon Air Temperature (CAT) model (Erell and Williamson 2006). However, the sol-air temperature does not account for the thermal properties of the sub-surface material, including the thermal conductivity and heat capacity, both of which may be affected by soil moisture. It also fails to account for the effects of latent heat flux at the surface (mostly evaporation but sometimes condensation in the form of dew).

There are several methods to estimate sensible, latent, and storage heat fluxes from a moist surface—either vegetated or saturated bare soil. Penman (1948) combined an aerodynamic approach with the surface energy balance to estimate evaporation from a wet surface without knowing the surface temperature. Monteith (1965) subsequently added the effects of partially closed stomata to calculate evapotranspiration from water-stressed vegetation in what is known as the Penman–Monteith equation. Shuttleworth and Wallace (1985) further developed this equation to represent sparse crops by means of the Leaf Area Index (LAI), which enabled them to partition the effect of vegetation and the effect of bare soil while maintaining a one-dimensional representation of the fluxes.

Deardorff (1978) proposed a parameterization of surface temperature which includes a representation of a vegetation canopy layer interacting with both its underlying soil layer and the atmosphere above it. This model operates by solving energy balance equations for a bare soil surface and for a full cover vegetation canopy and by correlating the heat fluxes between these cases for a partially vegetated surface. The correlation includes fluxes of moisture and heat from both the canopy and the underlying soil to the air space within the canopy. The air space within the canopy is then used to calculate these fluxes to the atmosphere.

Best (1998) proposed a simplification of Deardorff's model of vegetation that would nonetheless result in a minimal loss of accuracy. This model assumes that the turbulent transfer between the vegetation and the soil is much smaller than the turbulent transfer into the atmosphere. By neglecting the turbulent fluxes between the vegetation and the soil for dense vegetation, the internal canopy air temperature and humidity are no longer required. The fluxes of heat and moisture into the atmosphere can then be calculated directly from the vegetation properties. This allows Best's Portable Surface Temperature (POST) model to be used in various settings with inputs that are available at a standard weather station.

Liang et al. (1994) described an energy flux model that is comprised of a two-layer characterization of the soil column and uses an aerodynamic representation of the latent and sensible heat flux at the land surface. The algorithm can account for soils with varying infiltration capacities and allows for different types of vegetation to be represented simultaneously. The actual evapotranspiration from each vegetation type is characterized by potential evapotranspiration, together with canopy resistance, aerodynamic resistance to the transfer of water, and physical resistance. The upper soil layer is defined so as to respond to rainfall events, and the lower soil layer is used to characterize the slowly varying soil moisture behavior. The ground heat flux is estimated using two thermal soil layers. The first soil layer has a varying daily temperature at the interface with the second layer which is required as an input for the model. The second (deeper) soil layer is characterized by constant soil temperature as the bottom boundary condition. The heat storage in the first soil thermal layer is assumed to be negligible. The model is formulated as a fully coupled water and energy balance system.

The Fast All-Season Soil Strength (FASST) model (Frankenstein and Koenig 2004) calculates the energy and water budget from a vegetated surface using a comprehensive multi-layer description of the soil. It quantifies both the flow of heat and moisture within the soil and also the exchange of heat and moisture at all interfaces (ground–air or ground–snow; snow–air) using both meteorological and terrain data. FASST is a very detailed model, suitable for users who have a full description of their site, and allows thermal and hydrological analysis of several terrain types including asphalt, concrete, bed rock, permanent snow, or low vegetation such as grasses, shrubs, marsh, tundra, and desert vegetation. At a minimum, the only meteorological data required is air temperature, but model performance with such limited inputs is not validated.

The objective of this research is to propose a relatively simple formulation for urban micrometeorological models that is simpler to apply than FASST or the Liang et al. method, yet which accounts for the changing thermal properties of soils in response to variations in moisture content, as well as a simplified means of describing the effect of surface cover vegetation, such as grass. The model should be capable of calculating the hourly surface temperature using only widely available data from a standard meteorological station (namely air temperature, incoming radiation, precipitation, and vapor pressure) and inputs that characterize the ground such as albedo, thermal conductivity, heat capacity, and infiltration capacity. It should require no a priori knowledge of soil temperature or moisture at any depth.

2 Methods

2.1 Model development

The vegetated/permeable surface energy balance (VP-SEB) model is based on a surface energy balance formulation combining several equations from various sources. Foremost, among these is the ground storage flux formulation proposed by Liang et al. (1994), which uses a two-layer characterization of the soil column with a prescribed boundary condition at each ground level. The sub-surface temperature is obtained using a sinusoidal function proposed by Hillel (1982), for annual and diurnal cycles. The latent heat flux is estimated using the Penman–Monteith equation (Penman 1948; Monteith 1965). A simplified procedure to describe changing soil moisture content is proposed, which then affects the latent heat flux and, in turn, the surface temperature. The energy fluxes are a function of the surface temperature itself, so an iterative procedure is used to solve the SEB equations.

The energy balance of a surface is described by the following general equation:

$$Q^{*} = Q_{\mathrm{H}} + Q_{\mathrm{E}} + \Delta Q_{\mathrm{S}} \tag{2}$$

where Q^{*} (W m^{-2}) is the net radiative flux, Q_{H} (W m^{-2}) is the sensible heat flux, Q_{E} (W m^{-2}) is the latent heat flux, and ΔQ_{S} (W m^{-2}) is the change in energy stored in the soil.

2.1.1 Sensible heat flux

The sensible heat flux (Q_{H}) represents the energy exchange between a surface and its adjacent air and is proportional to the difference between the surface temperature (T_{s}, K) and the air temperature at screen height (T_{a}, K). This difference is multiplied by the convective heat transfer coefficient (h_{c}, W m^{-2} K^{-1}) which depends mainly on wind velocity and turbulence. The heat transfer coefficient is obtained empirically and is affected by the specific heat and density of air [C_{p} (J kg^{-1} K^{-1}) and ρ_{a} (kg m^{-3}), respectively] and the aerodynamic resistance (r_{a}, s m^{-1}) which is a function of wind speed and the stability status of the atmosphere.

The sensible heat flux is described as follows:

$$Q_{\mathrm{H}} = h_{\mathrm{c}}(T_{\mathrm{s}} - T_{\mathrm{a}}) = \frac{\rho_{\mathrm{a}} C_{\mathrm{p}} (T_{\mathrm{s}} - T_{\mathrm{a}})}{r_{\mathrm{a}}} \tag{3}$$

Rearranging Eqs. (2) and (3) gives the surface temperature

$$T_{\mathrm{s}} = T_{\mathrm{a}} + \frac{r_{\mathrm{a}}\left(Q^{*} - Q_{\mathrm{E}} - \Delta Q_{\mathrm{S}}\right)}{\rho_{\mathrm{a}} C_{\mathrm{p}}} \tag{4}$$

Air temperature is obtained from the meteorological time series, but the remaining terms depend on the surface temperature as well, so an iterative scheme is used to obtain them.

There are numerous expressions relating the convective heat transfer coefficient to wind speed above the surface. As the intended application of VP-SEB is in studies of urban micrometeorological conditions, the expression proposed by Hagishima and Tanimoto (2003) was considered the most appropriate

$$h_{\mathrm{c}} = 3.96\sqrt{u^2 + v^2 + w^2} + 6.42 \tag{5}$$

where u, v, and w (m s^{-1}) are the wind speed components at 0.13 m above the surface. In the case of a relatively large exposed surface, it may be possible to neglect the v and w components without compromising accuracy substantially.

Wind speed adjacent to the surface is obtained from the meteorological record using the transformation proposed by Macdonald (2000). Equation (6), which was derived from wind tunnel data, gives the relation between wind speed at two given heights, accounting for three-dimensional surface obstacles (cubes) which could be representative of a simple urban-type surface. The frontal density (λ_{f}), which is the ratio between the frontal area of each obstacle exposed to wind and the underlying surface area of the obstacle, governs the change of wind speed with height

$$U_{0.13} = U_{10}\exp\left(9.6\lambda_{\mathrm{f}}\left(\frac{0.13}{10} - 1\right)\right) = U_{10}\exp(-9.4752\lambda_{\mathrm{f}}) \tag{6}$$

2.1.2 All-wave radiation

The net radiative flux of a surface (Q^{*}, W m^{-2}) is the sum of the net shortwave (solar) radiation and the net longwave radiation. It can also be represented as the sum of the radiative forcing (Q', W m^{-2}) and the emitted longwave radiation ($L_{\uparrow}$, W m^{-2}) (Eq. (7)). (Fluxes that exit the surface are considered negative and inward energy flow positive). The radiative forcing is governed by the intensity of the sun and by the temperature of the sky, as well as the albedo of the surface and its infrared absorptivity. The radiation emitted from the surface is given by the Stefan–Boltzmann law (Eq. (8)).

$$Q^{*} = Q' - L_{\uparrow} = \left(K_{\downarrow} - K_{\uparrow} + L_{\downarrow} - L_{refl}\right) - L_{\uparrow} \tag{7}$$

$$L_{\uparrow} = \varepsilon_{\mathrm{s}} \sigma T_{\mathrm{s}}^{4} \tag{8}$$

$$K_{\uparrow} = \alpha K_{\downarrow} \tag{9}$$

$$L_{refl} = (1 - \varepsilon_{\mathrm{s}}) L_{\downarrow} \tag{10}$$

where $K_{\downarrow}$ (W m^{-2}) and $L_{\downarrow}$ (W m^{-2}) are the incoming shortwave and longwave radiation, respectively, which are available from the meteorological time series; ε_{s} is the emissivity of the surface; σ (W m^{-2} K^{-4}) is the Stefan–Boltzmann constant (5.67 × 10^{-8}); L_{refl} (W m^{-2}) is the reflected longwave radiation; and $K_{\uparrow}$ (W m^{-2}) is the solar radiation reflected from the surface, depending on its albedo (α). Typical values for the surface albedo vary between 0.05 and 0.4.

The albedo of the soil (α) is also affected by moisture, with dry soils typically displaying a higher albedo. The increase in albedo with moisture is estimated by an expression following the general form proposed by Sugathan et al. (2014):

$$\alpha_{\mathrm{dry}} = \alpha_{saturated} + C_1 \times \exp(-\theta_0/C_2) \tag{11}$$

where θ_0 is the soil moisture content and C_1 and C_2 are the empirical constants.

2.1.3 Ground storage

The ground heat flux is obtained by solving the heat diffusion equation with a prescribed boundary condition at the bottom of the solution domain. Figure 1 shows a schematic representation of the ground temperature profile, which consists of two soil layers with depths z_{mid} (m) and z_{deep} (m), respectively. At depth z_{deep}, the soil temperature variations are assumed to be negligible on a diurnal cycle, and the temperature at this depth is represented by T_{deep} (K). The temperature T_{mid} (K) at depth z_{mid} changes throughout the day.

Liang et al. (1994) described the ground heat flux by combining the representation of fluxes at each thermal soil layer. The first soil layer with depth z_{mid} is described using the thermal conductivity (λ) and the temperature at the bottom of this depth (T_{mid}), while heat storage is considered negligible

$$\Delta Q_{\mathrm{s}} = \frac{\lambda}{z_{\mathrm{mid}}}\left(T_{\mathrm{s}} - T_{\mathrm{mid}}\right) \tag{12}$$

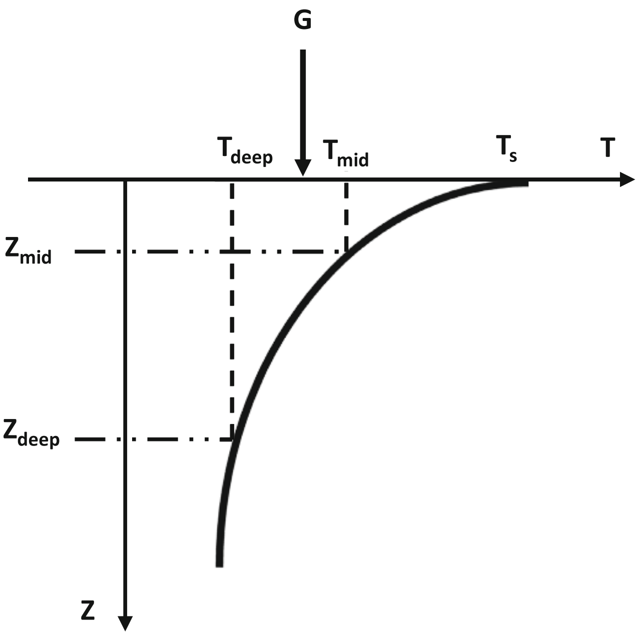

Fig. 1 Schematic representation of the sub-surface temperature profile (illustrated for the daytime). Diurnal variations decrease with depth

For the second layer with depth z_{deep}, the heat capacity (Cv) and thermal conductivity (λ) of the soil are used together with the intermediate soil temperature at the end and the beginning of a time step (T^{+}_{mid} and T^{-}_{mid}, respectively)

$$\frac{Cv\left(T^{+}_{\mathrm{mid}} - T^{-}_{\mathrm{mid}}\right)}{2\Delta t} = \frac{\Delta Q_{\mathrm{s}}}{z_{deep}} - \frac{\lambda\left(T_{\mathrm{mid}} - T_{deep}\right)}{z^2_{deep}} \tag{13}$$

The volumetric heat capacity and soil thermal conductivity depend on water content (θ_0, vol/vol), which will vary with depth. If the water table is very high, soil moisture may increase with depth. However, it is assumed here that the source of moisture is precipitation (or irrigation), so that moisture will decrease with depth and, beyond a certain depth, will remain at an equilibrium typical to the region. VP-SEB requires inputs of these properties for the dry soil and applies simplified relationships to fit experimental values reported by de Vries (1963) for different soil types.

The volumetric heat capacity is estimated as

$$Cv_{\mathrm{s}} = Cv_{\mathrm{s\_dry}} + (4.186 \times \theta_0) \tag{14}$$

The thermal conductivity is estimated as

$$\lambda_{\mathrm{s}} = \lambda_{\mathrm{s\_dry}} + C_3 \times {\theta_0}^{C_4} \tag{15}$$

where C_3 and C_4 are empirical constants.

From Eqs. (12) and (13), the ground flux is expressed as

$$\Delta Q_{\mathrm{s}} = \frac{\frac{\lambda}{z_{deep}}\left(T_{\mathrm{s}} - T_{deep}\right) + \frac{Cv\, z_{deep}}{2\,\Delta t}\left(T_{\mathrm{s}} - T^{-}_{\mathrm{mid}}\right)}{1 + \frac{z_{\mathrm{mid}}}{z_{deep}} + \frac{Cv\, z_{\mathrm{mid}}\, z_{deep}}{2\,\Delta t\,\lambda}} \tag{16}$$

Equation (16) requires inputs for the intermediate and deep ground temperature. The VP-SEB model estimates these inputs using a sinusoidal function (Eq. (17)), following Hillel (1982). The deep ground temperature fluctuates on an annual cycle but is assumed to be constant during the course of a day. The intermediate temperature changes on a diurnal basis with intervals similar to the meteorological time series

$$T(z,t) = T_{\mathrm{avg}} + A_0 e^{-z/d} \sin\left[\omega(t - t_0) - \frac{z}{d}\right] \tag{17}$$

Equation (17) is applied differently for an annual or a daily time scale (note the change of units)

A_0 (K) is the amplitude of the sine function $(\mathrm{T_{max}} - \mathrm{T_{min}})/2$, which is half of the difference between the coldest and hottest day in a year (annual use) or hour in a day (diurnal use).

T_{avg} (K) is the daily or yearly averaged surface temperature. If the mean annual surface temperature is not available, the mean annual air temperature with an addition of 2° can be used (Hillel 1982).

ω (h^{-1}) or (day^{-1}) is the angular frequency ($\frac{2\pi}{P}$): $P = 365$ (days) (annual use) and $P = 24$ (h) (diurnal use).

t (h) or (days) is the unit of the time series.

t_0 (h) or (days) is the offset in hours (or days) to match the sine function to the actual measured oscillation. The yearly value is obtained for a specific geographic location by matching the sine function of daily-averaged air temperature to the results of Eq. (17). Once the value is estimated for a specific location, it can be used for shorter (or other) time periods.

d (m) is the damping depth given as $d = \sqrt{2\frac{\lambda/C}{\omega}}$.

z (m) is the desired depth.

The sinusoidal model has several characteristics: (1) the diurnal or annual temperature cycle is due to the fluctuating inputs of air temperature during a 24-h period (day/night) or during a year (summer/winter), (2) the amplitude of temperature fluctuations decreases with depth, and (3) transfer of heat down (or up) the soil levels takes time, so there is a lag in the peak temperature occurrence between different soil levels.

2.1.4 Latent heat flux

The latent heat flux is calculated using the Penman–Monteith equation

$$Q_E = \lambda_w ET = \frac{s(Q^* - \Delta Q_s) + \rho_a C_p \frac{(e_s - e_a)}{r_a}}{s + \psi\left(1 + \frac{r_s}{r_a}\right)} \tag{18}$$

where s (mb K^{-1}) is the slope of the saturation vapor pressure–temperature relationship, ψ (0.66 mb K^{-1}) is the psychrometric constant, r_s (s m^{-1}) is the surface resistance, r_a (s m^{-1}) is the aerodynamic resistance, and the product $\rho_a C_p$ is the volumetric heat capacity of the air (J m^{-3}). $e_s - e_a$ (mb) represents the vapor pressure deficit between a moist surface and the air: e_a (mb) is the vapor pressure at screen height from the meteorological time series, and e_s (mb) is the vapor pressure at the surface. Air adjacent to a wet surface is assumed to be saturated (Penman 1948; Monteith 1965).

The relationship between air temperature and saturation vapor pressure (e_s) is described by Eq. (19). The slope of the saturation vapor pressure curve (s) at a given temperature is given by Eq. (20) (Allen et al. 1998, based on Tetens 1930 and Murray 1967)

$$e_s = 6.108\exp\left[\frac{17.27T_a}{T_a + 237.3}\right] \tag{19}$$

$$s = \frac{4098\left[0.6108\exp\left(\frac{17.27T_a}{T_a + 237.3}\right)\right]}{(T_a + 237.3)^2} \tag{20}$$

2.1.5 Surface resistance

When simulating a vegetated surface, a value in the range of 50–70 (s m^{-1}) is used for r_s of plants such as grass which are photosynthetically active during the daytime. Crassulacean acid metabolism (CAM) plants may have much higher surface resistance, with values as high as 500. Typical values for r_s are shown in Table 1.

For a bare surface, r_s depends greatly on the structure and texture of the soil. The relationship between r_s and the soil water content in the top 1–5 cm, θ_0 (m^3 m^{-3}), is usually formulated with an exponential function, since surface resistance increases substantially as the soil dries out.

2.1.6 Soil moisture content

Soil moisture content can be predicted from rainfall observations using an analytical method (Pan et al. 2003) which uses a time-dependent average of cumulative rainfall over a given period, typically at least 14 days, without knowing the diffusion rate of water into the soil. The initial conditions of the soil using this method are not needed when calculating for longer periods of time.

In VP-SEB, soil moisture (θ_0) is estimated by means of a simplified balance that accounts for the effect of changes in soil moisture content through evaporation and precipitation

$$\theta_0 = \theta_0^- + \left((P^- - ET^-)\left(\frac{\gamma}{z}\right)\right) \tag{21}$$

where θ_0^- (m^3 m^{-3}) is the soil moisture content from the previous time step and P^- (m s^{-1}) and ET^- (m s^{-1}) are the precipitation and evapotranspiration from the previous time step, respectively. γ is a dimensionless empirical infiltration coefficient representing the unsaturated soil's ability to absorb any incoming water in a layer of depth z (m), with values between 0.0 for impervious surfaces such as concrete and 1.0 for loosely packed granular soils such as sand or highly porous soils such as peat. $ET^- = \frac{Q_E^-}{\lambda_w \rho_w}$, where λ_w (J kg^{-1}) is the latent heat

Table 1 Values of surface (or crop) resistance for different surface types (Monteith 1965; Oke 1987)

Surface	r_s (s m^{-1})	Source
Open water	0	Oke (1987)
Crops	50	
Forests	80–150	
Short grass	70	
Different types of grass		
Timothy and meadow fescue	50	Monteith (1965)
Rough pasture with some clover	50	
Ryegrass	50–110	
Alfalfa-brome mixture	40	

of vaporization of water and ρ_w (kg m^{-3}) is the density of water. Irrigation, if any, is treated as the equivalent amount of precipitation.

To account for the effect on evaporation of changes in soil moisture content, the latent heat flux obtained from the Penman–Monteith equation is multiplied by the moisture factor (M_s). For $\theta_0 > 0.25$, $M_s = 1.0$, allowing unrestricted evaporation. For $\theta_0 \leq 0.25$, $M_s = 4.0\ \theta_0$, progressively restricting water loss as the soil dries. This implies a linear relationship between the moisture factor (M_s) and the soil moisture, which is clearly a simplification: as oil moisture drops below field capacity, the decline in evaporation may be expected to be exponential. However, because the thickness of the soil layer that directly affects evaporation is small—z was fixed at 5 cm—model performance was not adversely affected. Soil moisture (θ_0) is limited (arbitrarily) to a minimum value of 0.02 and a maximum value that depends on the porosity of the soil, which is about 0.4 for most soils but which may be as high as 0.8 for peat.

An estimate of the initial soil moisture content is used for a spin-up period. The sensitivity of the model to the accuracy of this estimate declines with spin-up time, the length of which depends on the rate of evaporation and the frequency and magnitude of subsequent precipitation events. However, a spin-up period of several days may be required if the initial estimate differs substantially from the actual value of soil moisture.

2.2 Calculation procedure

1. Parameters that do not depend on surface temperature ($L_\downarrow$, $K_\downarrow$, Q', $U_{0.13}$, h, r_a, s, e_s) are calculated using the atmospheric input parameters. These parameters will stay constant throughout the iteration (Fig. 2).
2. T_{mid} and T_{deep} are calculated for the entire desired period.
3. The energy terms ΔQ_S, Q^*, and Q_E, which also depend on the surface temperature, are calculated using the air temperature for the first iteration.
4. The surface temperature is calculated using Eq. (22), obtained by isolating the surface temperature term from Q_H

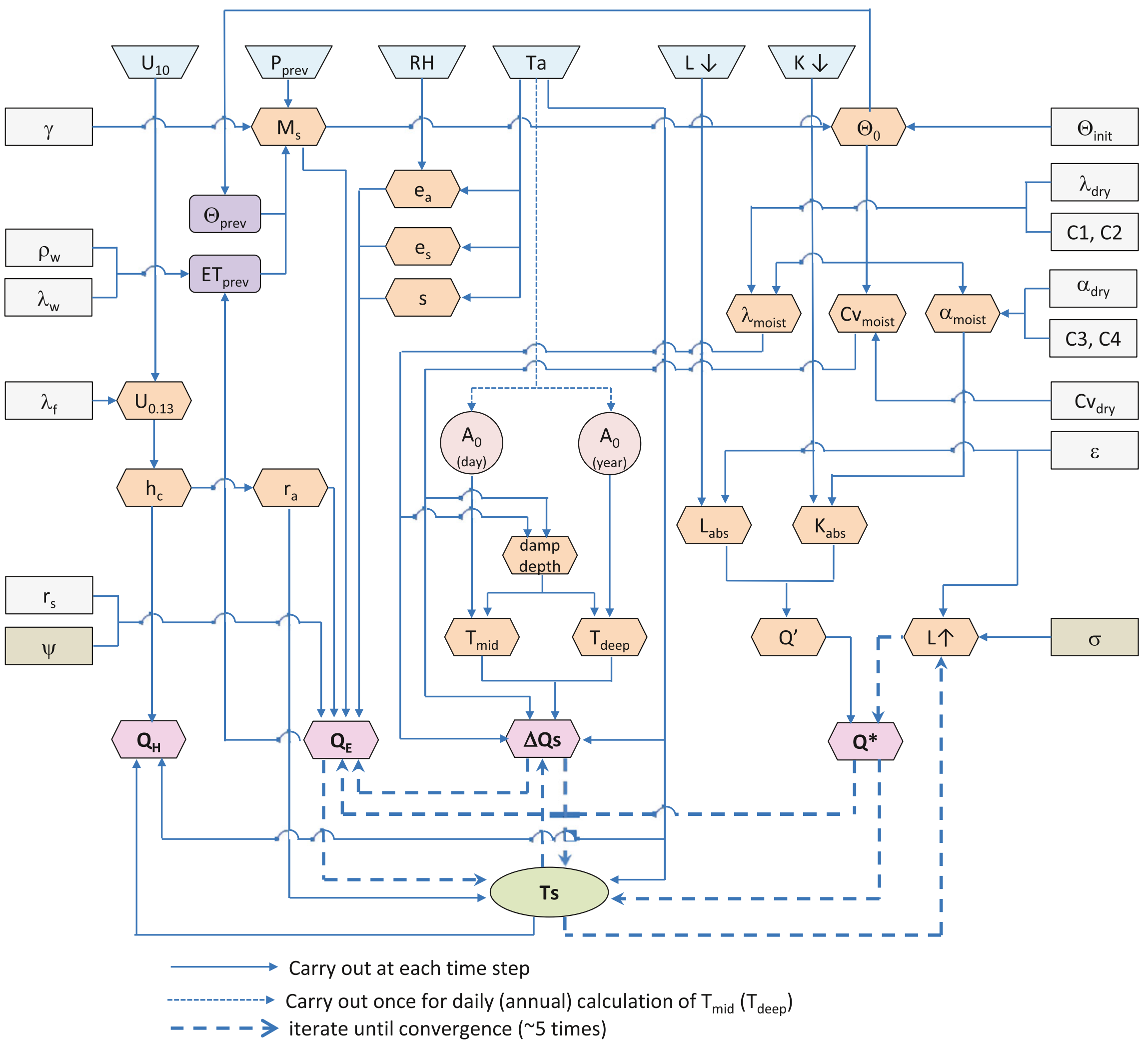

Fig. 2 Flow chart of the VP-SEB calculation procedure

and ΔQ_s in the energy balance equation following Liang et al. (1994)

$$T_s = \frac{Q^* - Q_E + \frac{\rho C_p T_a}{r_a} + \frac{\frac{\lambda}{z_{deep}} T_{deep} + \frac{C_v z_{deep}}{2 \Delta t} T_{mid}}{1 + \frac{z_{mid}}{z_{deep}} + \frac{C_v z_{mid} z_{deep}}{2 \Delta t \lambda}}}{\frac{\rho C_p}{r_a} + \frac{\frac{\lambda}{z_{deep}} + \frac{C_v z_{deep}}{2 \Delta t}}{1 + \frac{z_{mid}}{z_{deep}} + \frac{C_v z_{mid} z_{deep}}{2 \Delta t \lambda}}} \quad (22)$$

5. The soil moisture content (θ_0) and M_s are updated using the calculated evapotranspiration.
6. Steps 2 to 5 are repeated using the estimated surface temperature from the previous iteration until the surface temperature converges (Fig. 2). Experience suggests that the procedure converges rapidly, and four to five iterations are sufficient.

The entire calculation is implemented in FORTRAN. The code is provided as supplementary material to this paper, as well as a sample input file.

2.3 Validation with observational data

The VP-SEB model was validated against the surface temperature of a loess soil surface under various weather conditions at the Sde Boqer meteorological station for a period of 1 year (2014) (Fig. 3). Meteorological inputs required for VP-SEB were taken from the same meteorological station (http://bidr.bgu.ac.il/BIDR/research/phys/meteorology/default.asp).

Sde Boqer is in the arid Negev desert of Israel at 30.8° N latitude, approximately 480 m above sea level. The climate is characterized by sharp daily and seasonal thermal fluctuations, dry air, and clear skies with intense solar radiation. During the hot and dry summers, the mean daily maximum air temperature is approximately 33 °C, while nights dip to an average of 18 °C. Winter days are typically cool and sunny with daily mean air temperature of 14.4 °C and a nightly minimum of 3.8 °C. Prevailing winds are northwesterly and moderately strong during the late afternoon and evening (Bitan and Rubin 1994).

The soil at Sde Boqer may be characterized as a clay loam. The dry soil has a thermal conductivity of about 0.3 W m^{-1} K^{-1} and a volumetric heat capacity of 1.4 MJ m^{-3} K^{-1}. Soil albedo is 0.39 when dry (Snir et al. 2016) and 0.24 when wet. The organic content of the soil is negligible, and it has a very low infiltration coefficient, so that surface runoff is generated very easily following rain events of modest volume and intensity, even if the soil at a depth of several centimeters below the surface is not saturated.

Model inputs for Sde Boqer are shown in Table 2.

The model was also validated against surface temperature data for grass and asphalt, both obtained by infrared imaging (infrared thermometer, IRT) for periods of several hours on a mild spring day and a hot summer day at the Sde Boqer Campus (Snir et al. 2016).

Fig. 3 Landscape at Sde Boqer

3 Results and discussion

3.1 Statistical analysis

The quality of the modeled surface temperature was assessed by comparison of the predicted and observed values using regression analysis, error analysis, and goodness-of-fit tests.

Moriasi et al. (2007) noted that model output is compared to corresponding measured data with the assumption that all

Table 2 Inputs used for the Sde Boqer validation test

Parameter	Value
Soil albedo, saturated (dry)	0.24 (0.39)
Constants for albedo correction (C_1, C_2)	0.15, 0.15
IR emissivity of soil	0.90
Heat capacity of dry soil (MJ m^{-3} K^{-1})	1.35
Thermal conductivity of dry soil (W m^{-1} K^{-1})	0.50
Constants for conductivity correction (C_3, C_4)	2.1, 0.55
Soil infiltration coefficient	0.2
Soil initial moisture content (vol vol^{-1})	0.15
Bulk density of dry soil (kg m^{-3})	1600
Offset of minimum air temperature (days)	105
Soil moisture maximum (vol vol^{-1})	0.4
Mean annual air temperature (°C)[a]	21.4
Annual amplitude of mean daily air temperature (°C)[a]	14.6

[a] These values are also calculated by the software if the weather (input) file describes an entire year

error variance is contained within the predicted values and that observed values are error free. As this is not the case in observations of earth–atmosphere interactions, they recommend that in addition to graphical techniques and standard performance measures, three quantitative statistics should be used: the Nash–Sutcliffe efficiency (NSE), percent bias (PBIAS), and the ratio of the root mean square error to the standard deviation of measured data (root-mean-square error, RSR). The Nash–Sutcliffe Efficiency Index defines the proportion of the initial variance within the observed data accounted for by the model (Nash and Sutcliffe 1970) and ranges between −∞ and 1.0, with NSE = 1 being the optimal value. PBIAS measures the average tendency of the simulated data to be larger or smaller than their observed counterparts (Gupta et al. 1999), with an optimal value of 0.0. RSR standardizes the root-mean-square error using the observations standard deviation and has an optimal value of 0.0.

In numerous situations, the value (v) of an input variable (or a combination of several variables) can provide a fairly close approximation to the measured parameter (m). A model may only be considered useful if the estimated value of the parameter in question (e) is closer to the observed value than this trivial approximation of the input variable. According to the Williamson degree of confirmation (Williamson 1995), a model will be considered suitable if the predicted value (in this case, modeled surface temperature) will provide a better fit to the measured value than an arbitrary estimate such as the input value (in this case, measured air temperature). The indicator varies from −∞ to 1.0, with values between 0.0 and 1.0 indicating an improvement relative to the arbitrary reference. This indicator is used in addition to the standard measures and the more sophisticated ones recommended by Moriasi et al. (2007), Willmott (1981, 1982), and Willmott et al. (1985).

Statistical measures of model performance are shown in Table 3.

Table 3 Statistical evaluation of the predicted surface temperature

Total number of hours	8760
Mean error	0.68
Standard deviation of error	2.68
Maximum error	10.54
Minimum error	−11.22
Root mean square error	2.77
Systematic root mean square error	0.68
Unsystematic root mean square error	2.68
Willmott index of agreement	0.99
Williamson degree of confirmation	0.73
Nash–Sutcliffe Efficiency Index	0.95
Percent bias (PBIAS)	2.72
RMSE-observed std. dev ratio (RSR)	1.03

3.2 Visualization of results and statistics

3.2.1 Annual cycle of sub-soil temperature at a depth of 30 cm

The sub-surface temperature at a depth of 30 cm, modeled by VP-SEB to estimate the ground storage flux (Eq. (17)), was compared with measured values from the Sde Boqer weather station. Figure 4 shows the evolution of this temperature over the course of a year. Modeled values show a small positive bias in summer and a small negative bias in winter, but the error is typically less than 2 K. The measured data display two instances of a rapid drop in value, in March and May, both of which are the result of substantial precipitation events. The Hillel model does not account for such phenomena, but the resultant error in the modeled surface temperature due to this discrepancy is small (see Figs. 6 and 7).

3.2.2 Regression analysis of surface temperature

The modeled surface temperature for the entire year is compared with observational data (Fig. 5), showing good agreement overall with a best-fit regression line having a slope close to unity and a negligible offset.

3.2.3 Time series for cold wet weather and hot dry weather periods

Model performance is illustrated in detail for two periods of several days each. Figure 6 shows an early spring period beginning with several dry, sunny days followed by overcast weather and a major storm that deposited 20 mm of rain over a 2-h period on March 7, providing a good test of model sensitivity to changing weather and variations in soil moisture content. Changes in soil moisture and the latent flux following

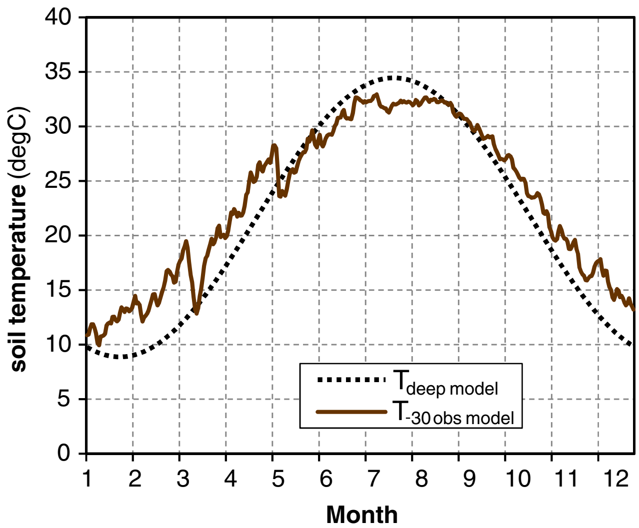

Fig. 4 Annual evolution of the mean daily sub-surface soil temperature at a depth of 30 cm

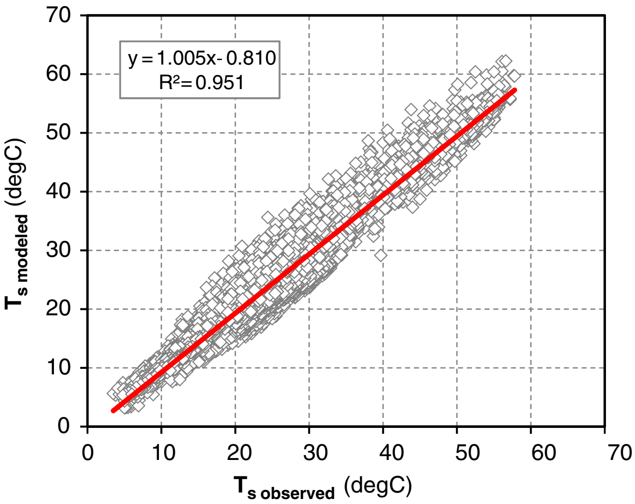

Fig. 5 *X–Y* plot showing hourly observed and modeled surface temperature for 2014 (8760 hourly values)

the rain are reflected in model output, as the surface temperature over the subsequent days is substantially lower than in the preceding period. The latent heat flux following the rain event remains moderate at first and increases substantially only once the daytime radiant flux is sufficient to generate substantial evapotranspiration. Figure 7 shows a hot dry summer period during which the soil is completely dry. During the daytime, modeled surface temperature is generally in good agreement with observations, while at night, there is a small negative bias. The latent heat flux during this period is extremely low.

3.2.4 Time series for asphalt and grass

In addition to soils, VP-SEB was designed to support modeling of the surface temperature of pavement and ground cover vegetation. In the absence of suitable long-term surface temperature data, short-term observations by an IRT were used. Although the number of data points is too small to support statistical analysis, Fig. 8 demonstrates that in principle, given appropriate inputs, the model is capable of reproducing the diurnal surface temperature pattern with acceptable accuracy. Grass surface temperature remains only a little above air temperature for most of the day (top left) and the intense sunlight offset by evapotranspiration (bottom left). Once solar radiation levels drop in the afternoon, the small grass patch is even a little cooler than the hot dry air advected from the surrounding desert. On the right, the asphalt surface temperature measures nearly 25° warmer than the air around noon (top), as most of the incoming solar radiation is absorbed in the pavement (bottom right).

3.3 Sensitivity analysis

Soil characteristics at a given location may not always be known precisely. Sensitivity analysis is used to assess the effect of inaccurate data for volumetric heat capacity, thermal conductivity, soil infiltration, and albedo on predicted surface temperature. Results of the analysis are shown in Table 4, showing the base values (in italics) of the analysis (for loess

Fig. 6 Time series showing temperature (*top*) and fluxes (*bottom*) for a 5-day period in spring (March 6–10, 2014; all values were generated by the VP-SEB model except T_{a_obs} and T_{s_obs})

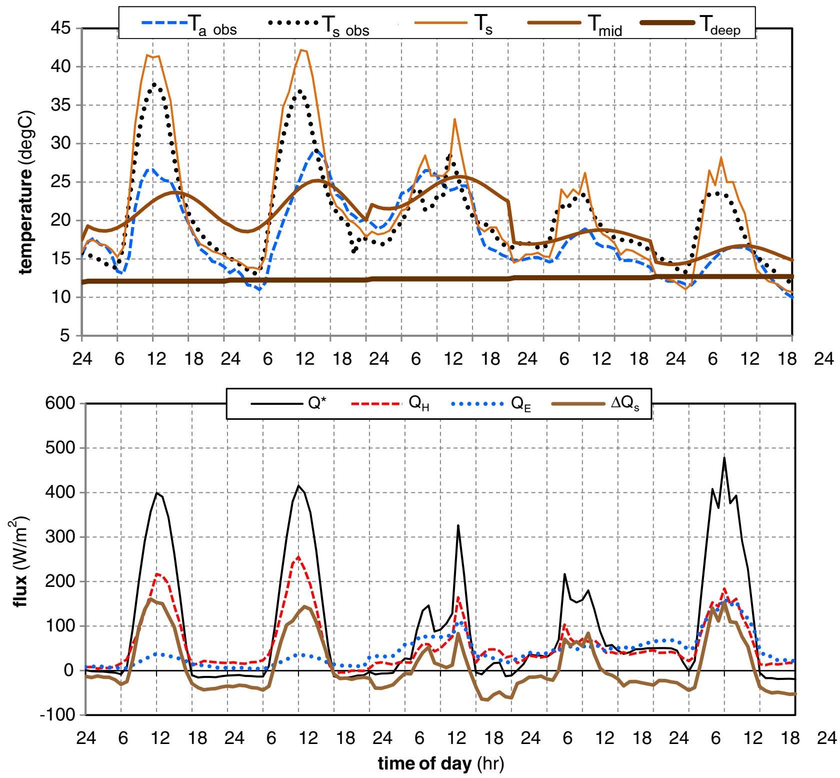

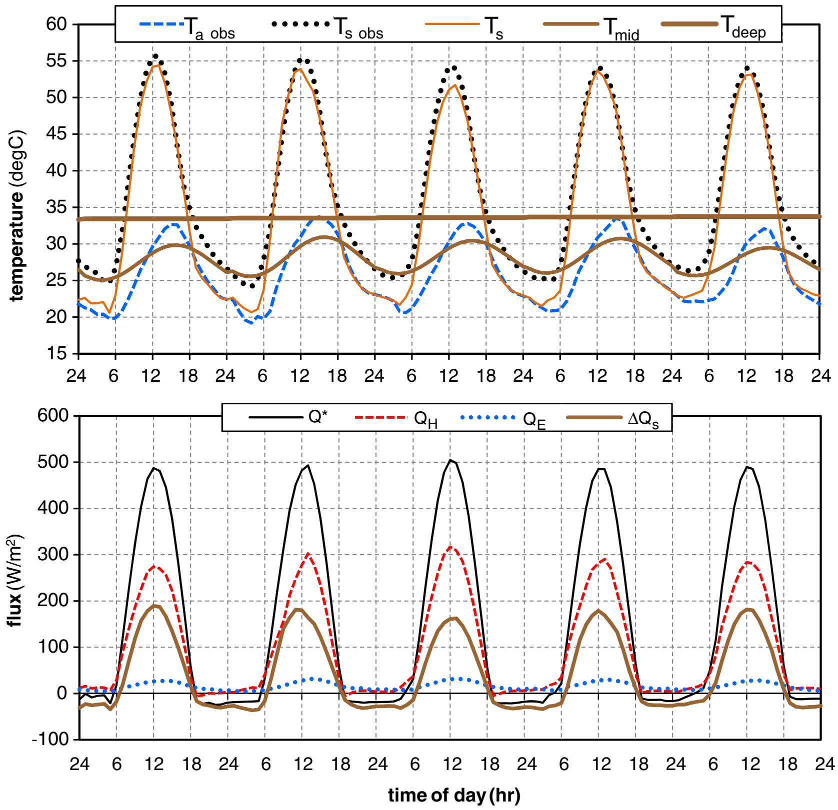

Fig. 7 Time series showing temperature (*top*) and fluxes (*bottom*) for a 5-day period in summer (July 1–5, 2014; all values were generated by the VP-SEB model except T_{a_obs} and T_{s_obs})

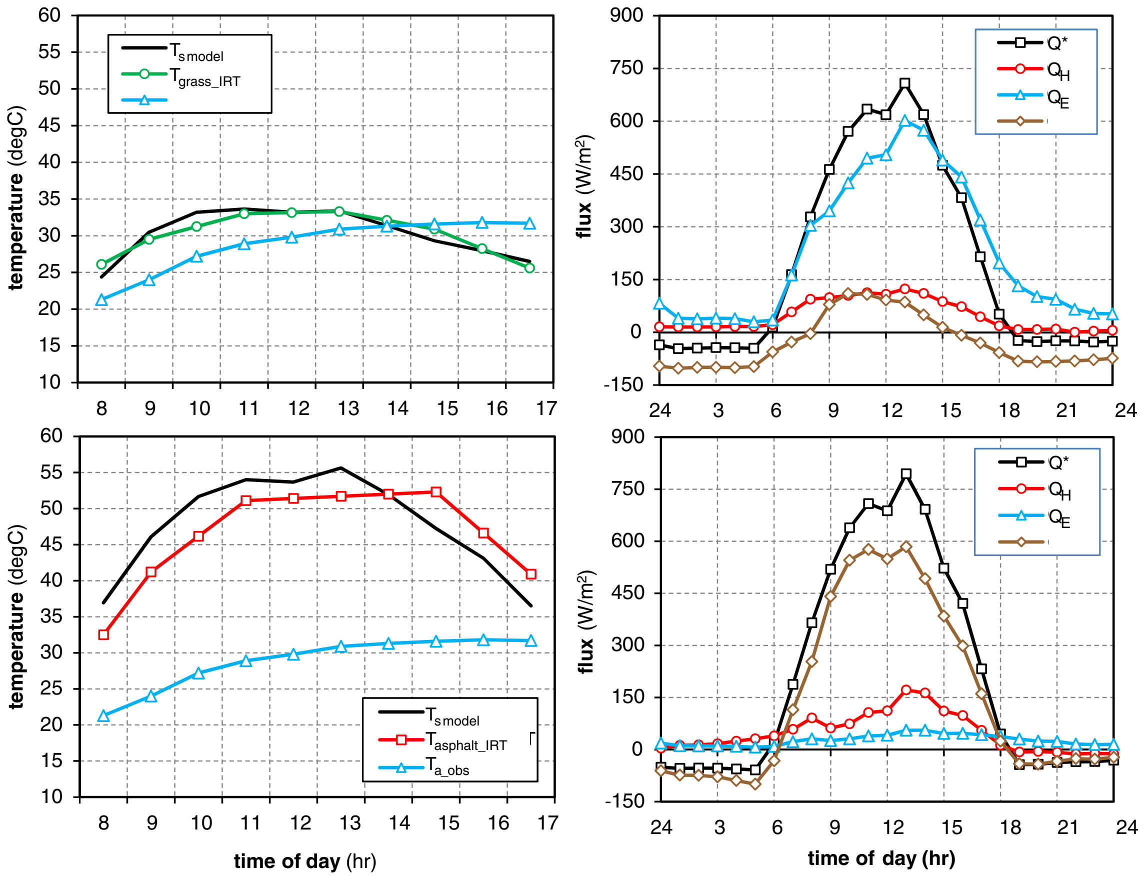

Fig. 8 Time series showing temperature (*left*) and fluxes (*right*) at Sde Boqer for a small grass plot (*top*) and for a weathered asphalt road (*bottom*). (Measured data are from Snir et al. 2016)

Table 4 Sensitivity analysis of the VP-SEB model using the Sde Boqer data

Parameter	Value	% change	Mean error	std dev	Williamson DoC	Nash–Sutcliffe
Volumetric heat capacity (mJ m^{-3} K)	0.68	−50	0.62	2.90	0.715	0.937
	1.35	*0*	*0.68*	*2.68*	*0.734*	*0.945*
	2.03	+50	0.70	2.67	0.742	0.949
Thermal conductivity (W m^{-2} K)	0.25	−50	0.38	3.09	0.703	0.931
	0.50	*0*	*0.68*	*2.68*	*0.734*	*0.945*
	0.75	+50	0.92	2.45	0.746	0.951
Infiltration coefficient	0.10	−50	0.75	2.63	0.737	0.947
	0.20	*0*	*0.68*	*2.68*	*0.734*	*0.945*
	0.30	+50	0.67	2.72	0.731	0.944
Albedo (dry surface)	0.20	−50	−1.00	4.28	0.594	0.861
	0.29	−25	−0.21	3.44	0.676	0.915
	0.39	*0*	*0.68*	*2.68*	*0.734*	*0.945*
	0.49	+25	1.57	2.34	0.723	0.943
	0.59	+50	2.46	2.58	0.641	0.909

soil) which are used as the baseline (see also Table 1). Improved model predictions are reflected by a lower standard deviation of the error, a higher Williamson degree of confirmation, and a higher Nash–Sutcliffe Efficiency Index.

As the table shows, prediction of surface temperature is very sensitive to changes in albedo. Sensitivity to thermal conductivity and volumetric heat capacity is much lower. The sensitivity to the infiltration coefficient of the soil also appears to be low, but this may reflect the fact that Sde Boqer soil is typically dry and precipitation events infrequent.

4 Application in pedestrian thermal comfort

To simulate the effect of vegetation on pedestrian thermal stress, the VP-SEB model was run for an asphalt surface and for a vegetated surface. A negligible value of soil moisture is taken for asphalt while the grass is assumed to be well irrigated.

Thermal comfort may be described by the Index of Thermal Stress (ITS), which expresses the overall energy exchange between a human body and its surrounding environment. The ITS is adjusted for urban surroundings and expresses the latent heat of sweat evaporation that is required for a human body to maintain a thermal equilibrium with the environment (Givoni 1963; Pearlmutter et al. 2007)

$$\mathrm{ITS} = \frac{R_n + C + (M - W)}{f} \tag{23}$$

$$R_n = (K_{dir} + K_{dif} + \alpha_h K_h + \alpha_v K_v)(1 - \alpha_s) + L_d + L_h + L_v - \varepsilon_s \sigma T_s^4 \tag{24}$$

where R_n is the net radiation for a body, C is the heat convection from a body, M-W is the net internal body heat production accounting for metabolism (M) and work (W), and f is the efficiency of sweat evaporation. K is the shortwave solar radiation (direct and diffuse); αK is the reflected shortwave radiation (from horizontal and vertical surfaces); α_s is the body surface albedo; L is the longwave radiation emitted from the surfaces (downwards, horizontally, and vertically). ε_s and T are the surface emissivity and temperature of the body. The energy value of ITS (watts) is correlated with a subjective thermal sensation scale based on surveys: *comfortable* (ITS < 160, *warm* (160 < ITS < 480), *hot* (480 < ITS < 800), and *very hot* (ITS > 800).

The inputs for the ITS model include the location and time of day (required to calculate the sun position), building heights and street width, hourly meteorological data, and surface temperature. A time series of the ITS was generated in order to evaluate the effect of replacing an asphalt surface with a vegetated surface.

Figure 9 shows the effect on pedestrian thermal stress of replacing asphalt pavement with grass in a hypothetical open space in hot, dry weather, as estimated by the ITS using the ground surface temperature shown in Fig. 8. As the figure shows, the combination of relatively high air temperature, moderate humidity, low wind speed, and intense sunlight results in hot conditions for an exposed pedestrian. However, a full plant cover was found to reduce the thermal stress on a pedestrian by as much as 100 W compared to a fully paved surface. These results agree with ITS values calculated from surface temperature measurements reported by Snir et al. (2016).

The reduction in thermal stress due to the planted surface in these meteorological conditions is equivalent to the effect of lowering the dry bulb air temperature by approximately 8 °C, all else being unchanged.

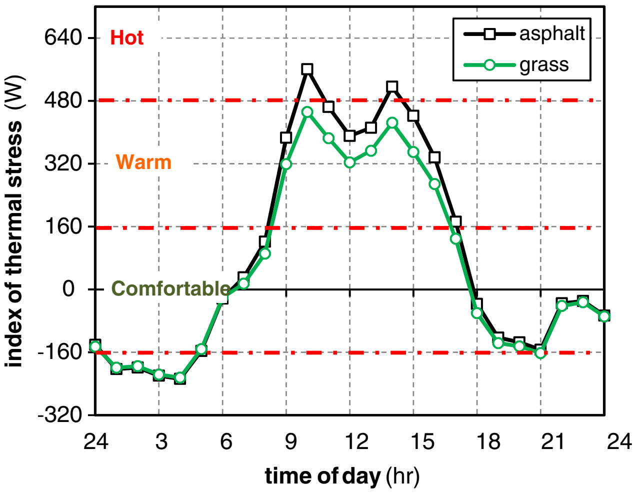

Fig. 9 The effect on pedestrian thermal stress of replacing asphalt with grass (ITS values of −160–160 W are considered "comfortable," 160–480 "warm," 480–800 "hot," and above 800 "very hot")

5 Discussion

VP-SEB is formulated to calculate surface temperature on small uniform patches of the urban surface and to support estimates of thermal comfort or building energy consumption at the scale of meters to tens of meters. Consequently, it does not incorporate spatial averaging of non-uniform surfaces. This is justified because horizontal fluxes of heat in the soil are negligible at this scale. In the case of a non-uniform environment, such surfaces must be resolved independently. Their overall effect may then be calculated using view factors and area-weighting schemes, as appropriate to the objectives of the procedure.

Solution of the surface energy balance requires wind speed near the surface. The heterogeneity of the urban area results in substantial variations in this datum in space and time, which are difficult to resolve even with the most sophisticated models. VP-SEB employs a simplified relationship (Eq. (6)) that does not account for the roughness of individual facets of the urban canyon and the presence of street furniture, trees, or automobiles. It also fails to account for variations in the shape of the velocity profile due to atmospheric stability conditions. However, such compromises were deemed acceptable in the absence of any practical alternative.

In most urban micrometeorological studies, the storage flux (ΔQ_s) is obtained as a residual once the other fluxes have been determined. This approach necessarily leads to closure of the surface energy balance: all errors in estimation of the other fluxes are reflected in this value. However, as Masson et al. (2002) noted, "closure of measured energy balances is rarely achieved over simple sites where micrometeorological theory is most likely to hold." VP-SEB estimates ΔQ_s directly from the difference between the deep soil temperature (obtained by means of the Hillel prognostic model) and the surface temperature, which is obtained from the iterative numerical process that satisfies the surface energy balance. However, this does not eliminate all possible errors, because of the simplified parametric procedures employed in VP-SEB. Therefore, although the overall error in the surface temperature is relatively small, there may still be discrepancies in some of the fluxes such that closure does not necessarily occur at all times.

Unlike most urban micrometeorological models, which are forced by atmospheric properties of the urban boundary layer, the forcing data required to run VP-SEB are obtained from a weather station in the vicinity, which measures near-surface conditions. This has the advantage of much better availability of the data, at the potential expense of errors introduced by intra-urban variability. This means that VP-SEB is best suited for integration in models of the urban street canyon, such as CAT, for which it was developed, or models such as the urban climate generator scheme proposed by Bueno et al. (2013), but not TEB (Masson 2000).

The application of VP-SEB is presently limited by the following restrictions:

a. Because modeling the ground storage flux requires an estimate of the soil temperature at a depth of 30 cm below the surface, based on the Hillel model, it cannot be applied where the sine form of this model does not apply—such as near the equator. This restriction may be relaxed in practice, if the sub-surface soil temperature in such regions is almost constant, by setting the annual amplitude of the temperature equal to zero, but this approach was not tested here.
b. VP-SEB cannot model snow or frozen soils.
c. VP-SEB employs a very rudimentary scheme to estimate soil moisture and assumes that all soil moisture originates locally, from precipitation or irrigation. Surface or subsurface flows of water are not modeled. Also not accounted for is moisture that may originate in a high water table.
d. Water loss by evapotranspiration is controlled only by the effect of solar radiation and wind and is not restricted by the changing hydraulic resistance of the soil as it dries. Water content at saturation is limited by pore space (about 40% for most soils) and is allowed to drop down to a minimum of 2%.
e. The coupling of the surface cover vegetation to the underlying soil substrate is assumed to occur by conduction only, via plant roots or direct contact of the foliage. VP-SEB does not model an intermediate air layer and is thus suited for modeling grass or ground-cover succulents but not bushes.

Validation of the VP-SEB model for an extended period was carried out using data from only one location. Although the goodness-of-fit tests for this location were satisfactory, the model will certainly benefit from evaluation using other data sets. In particular, a long-term record of the surface temperature of vegetation, such as grass, will improve confidence in the model's robustness for such surfaces.

6 Conclusions

The objective of this research was to develop a relatively simple model for the surface temperature of a permeable or vegetated surface using a physically based solution for the energy fluxes. The VP-SEB model requires only widely available data from a standard meteorological station and inputs that describe the surface—albedo, thermal conductivity, heat capacity, and infiltration capacity. It requires no a priori knowledge of soil temperature or moisture at any depth, nor does it require any other descriptors of the atmosphere. Rather, the surface temperature was modeled using an iterative procedure that combines a two-layer representation of the soil column with a sinusoidal function for calculating the ground flux, and a simplified procedure to describe changes in moisture content with a minimal loss of accuracy.

Statistical analysis showed that VP-SEB's modeled surface temperature is a close proxy of the measured data and is therefore suitable for analysis and integration in local-scale micrometeorological models. Application of the model was demonstrated in a simple scenario assessing the thermal stress on a pedestrian standing on either aged asphalt or grass. Although the albedo of both surfaces is low, the model indicates a substantial difference in surface temperature, which is then reflected in the Index of Thermal Stress.

Surface properties such as radiant temperature and albedo play an important role in determining the total thermal stress on a person. It is hardly new that the use of vegetation as a surface cover can reduce such stress in over-heated conditions. However, many of the prior studies on the effects of urban green are empirical and describe only one site and a limited range of vegetation. This study provides the basis for a method for quantifying these effects in a variety of environmental conditions, especially during elevated heat stress.

Acknowledgements This research was made possible with the support of the Jewish National Fund.

References

Allen R, Pereira L, Raes D, Smith M (1998) Crop evapotranspiration—guidelines for computing crop water requirements—FAO irrigation and drainage paper 56. FAO 56.

Best M (1998) A model to predict surface temperatures. Bound-Layer Meteorol 88:279–306

Bitan A, Rubin S (1994) Climatic atlas of Israel for physical and environmental planning and design. Ramot Publishing Company, Tel-Aviv University, Tel-Aviv

Bueno B, Norford L, Hidalgo J, Pigeon G (2013) The urban weather generator. J Build Perform Simul 6:269–281

De Vries D (1963) Thermal properties of soils. In: van Wijk W (ed) Physics of plant environment. North-Holland Publishing Company, Amsterdam, pp 210–235

Deardorff JW (1978) Efficient prediction of ground surface temperature and moisture, with inclusion of a layer of vegetation. J Geophys Res Oceans 83:1889–1903

Erell E, Williamson T (2006) Simulating air temperature in an urban street canyon in all weather conditions using measured data from a reference meteorological station. Int J Climatol 26:1671–1694

Frankenstein S., Koenig G. 2004. FASST vegetation models. ERDC/CRREL TR-04-25.

Givoni B (1963) Estimation of the effect of climate on man—development of a new thermal index. Technion-Israel Institute of Technology, PhD thesis, Haifa

Gupta H, Sorooshian S, Yapo P (1999) Status of automatic calibration for hydrologic models: comparison with multilevel expert calibration. J Hydrol Eng 4:135–143

Hagishima A, Tanimoto J (2003) Field measurements for estimating the convective heat transfer coefficient at building surfaces. Build Environ 38:873–881

Hillel D (1982) Introduction to soil physics. Academic, San Diego

Krayenhoff ES, Christen A, Martilli A, Oke TR (2014) A multi-layer radiation model for urban neighbourhoods with trees. Bound-Layer Meteorol 151:139–178

Lee H, Mayer H, Chen L (2016) Contribution of trees and grasslands to the mitigation of human heat stress in a residential district of Freiburg, Southwest Germany. Landsc Urban Plan 148:37–50

Liang X, Lettenmaier DP, Wood EF, Burges SJ (1994) A simple hydrologically based model of land surface water and energy fluxes for general circulation models. J Geophys Res-Atmos 99:14415–14428

Lindberg F, Holmer B, Thorsson S (2008) SOLWEIG 1.0—modelling spatial variations of 3D radiant fluxes and mean radiant temperature in complex urban settings. Int J Biometeorol 52:697–713

Macdonald RW (2000) Modelling the mean velocity profile in the urban canopy layer. Bound-Layer Meteorol 97:25–45

Mackey CO, Wright LT (1943) Summer comfort factors as influenced by the thermal properties of building materials. Transactions of the American Society of Heating and Ventilating Engineers 49:148

Masson V, Grimmond CSB, Oke T (2002) Evaluation of the town energy balance (TEB) scheme with direct measurements from dry districts in two cities. J Appl Meteorol 41:1011–1026

Masson V (2000) A physically-based scheme for the urban energy budget in atmospheric models. Bound-Layer Meteorol 94:357–397

Meier AK (1990–91) Strategic landscaping and air-conditioning savings: a literature review. Energy and Buildings 15-16:479–486

Monteith JL (1965) Evaporation and environment. Symp Soc Exp Biol 90:205–234

Moriasi DN, Arnold JG, Van Liew MW, Bingner RL, Harmel RD, Veith TL (2007) Model evaluation guidelines for systematic quantification of accuracy in watershed simulations. Trans Am Soc of Agric Biological Eng 50:885–900

Mueller E, Day T (2005) The effect of urban ground cover on microclimate, growth and leaf gas exchange of oleander in Phoenix, Arizona. Int J Biometeorol 49:244–255

Murray FW (1967) On the computation of saturation vapor pressure. J Appl Meteorol 6:203–204

Nash J, Sutcliffe J (1970) River flow forecasting through conceptual models part I—a discussion of principles. J Hydrol 10:282–290

Oke TR (1987) Boundary layer climates. Methuen, London

Pan F, Peters-Lidard C, Sale M (2003) An analytical method for predicting surface soil moisture from rainfall observations. Water Resour Res 39(11):1314. doi:10.1029/2003WR002142

Pearlmutter D, Berliner P, Shaviv E (2007) Integrated modeling of pedestrian energy exchange and thermal comfort in urban street canyons. Build Environ 42:2396–2409

Penman HL (1948) Natural evaporation from open water, bare soil and grass. Proceedings of the Royal Society of London, Series A Mathematical and Physical Sciences 193:120–145

Shashua-Bar L, Pearlmutter D, Erell E (2009) The cooling efficiency of urban landscape strategies in a hot dry climate. Landsc Urban Plan 92:179–186

Shashua-Bar L, Pearlmutter D, Erell E (2011) The influence of trees and grass on outdoor thermal comfort in a hot-arid environment. Int J Climatol 31:1498–1506

Shuttleworth WJ, Wallace JS (1985) Evaporation from sparse crops—an energy combination theory. Q J R Meteorol Soc 111:839–855

Snir K, Pearlmutter D, Erell E (2016) The moderating effect of water-efficient ground cover vegetation on pedestrian thermal stress. Landsc Urban Plan 156:1–12

Sugathan N, Biju V, Renuka G (2014) Influence of soil moisture content on surface albedo and soil thermal parameters at a tropical station. J Earth Syst Sci 123:1115–1128

Tetens O (1930) Uber einige meteorologische Begriffe. z. Geophys 6: 297–309

Williamson TJ (1995) A confirmation technique for thermal performance simulation models. Building Simulation ’95, August 14-16, 1995, Madison, Wisconsin, U.S.A

Willmott C (1982) Some comments on the evaluation of model performance. Bull Am Meteorol Soc 63:1309–1313

Willmott C, Ackleson S, Davis R, Feddema J, Klink K, Legates D, O’Donnell J, Rowe C (1985) Statistics for the evaluation and comparison of models. J Geophys Res 90:8995–9005

Willmott CJ (1981) On the validation of models. Phys Geogr 2: 184–194

Yilmaz H, Toy S, Irmak M, Yilmaz S, Bulut Y (2008) Determination of temperature differences between asphalt concrete, soil and grass surfaces of the city of Erzurum, Turkey. Atmosfera 21: 135–146

תקציר

התכנון ההנדסי שהיה נהוג בישראל במשך עשרות שנים, בדומה לנהוג בארצות רבות אחרות, ראה בנגר העילי העירוני מטרד או בעיה הדורשת פיתרון. בתכנון לקוי, מי הגשם עלולים לגרום להצפות של הכבישים, וחדירה של מים לתת-הקרקע סמוך ליסודות הבניינים עלולה להביא לפגיעה ביציבותם. מערכות הניקוז תוכננו בדרך כלל במטרה לאסוף את מרבית מי הגשם ולסלק אותם במהירות וביעילות האפשרית מהמרחב הבנוי. במרבית היישובים, מי הגשם מגיעים בסופו של דבר אל ערוצים טבעיים ומשם, לא אחת, אל הים. בשנים האחרונות התגבשה הבנה, בין היתר בעקבות מחקרים בחו"ל, כי רצוי לנקוט בתכנון עירוני רגיש למים (תר"מ), המבטא יעוד שונה למים ומיישם אמצעים אחרים לשם כך.

פוטנציאל הנגר העילי הבלתי מנוצל בערי ישראל מוערך ב-100-70 מיליון מ"ק בשנה. מים אלו הם משאב אשר בתכנון נכון ניתן להפיק ממנו תועלת. בראש ובראשונה, ניתן לאגום אותם ולהחדיר אותם אל מאגר מי התהום, אם אינם מזוהמים יתר על המידה. מערכות של ביו-פילטרים, המהוות את מושא המחקר של צוותי מחקר אחרים בפרויקט, מאפשרות לשמר חלק מהמים האלה. אולם בתכנון נכון, מי הנגר העילי עשויים גם לתרום לאיכות החיים של תושבי העיר: ניתן להשתמש בהם להשקיה של צמחייה בגנים עירוניים קטנים ובערוגות, בתנאי שמווסתים את מהירות הזרימה ומסיטים אליהם את המים בצורה מושכלת. הצמחייה עשויה לשפר את הנוחות האקלימית של הולכי רגל בשטחים הפתוחים הסמוכים, ולהפחית את צריכת האנרגיה של בניינים למיזוג אוויר. המחקר הנערך על ידי הצוות במכונים לחקר המדבר משתלב בתוכנית מקיפה המיועדת להביא ליצירת ערים רגישות מים בישראל אשר ייטיבו לנצל את המשאב הזה.

התרומה של צמחייה לנוחות התרמית של הולכי רגל בעיר ולהפחתת צריכת האנרגיה בבניינים תלויה במיני הצמחים, במיקום שלהם במרקם העירוני ובאופן שבו הם משולבים בשאר מרכיבי הרחוב. את הצמחייה אפשר לשלב במספר אופנים: בגינות ציבוריות או פארקים שכונתיים; ברחובות; בגינות הבניינים; או על גבי הבניינים עצמם, בעיקר בגגות. התכנון חייב להביא בחשבון הן את מאפייני הסביבה הבנויה והן את מאפייני האקלים, ובפרט את תפרוסת המשקעים: מספר ימי הגשם מועט, העוצמות לעיתים גבוהות מאוד, ובעיקר – ישנה תקופת יובש ארוכה וקשה מאוד הנמשכת מספר חודשים בשנה. האקלים בארץ שונה מאוד מהאקלים השורר באחדות מהערים החלוצות בתחום, כגון מלבורן שבאוסטרליה ופורטלנד בארה"ב. לכן אפשר שהכלים המשמשים את המתכננים שם לא יתאימו לצרכים בישראל.

מטרות הפרויקט שעליו אחראית הקבוצה שלנו הן אפוא: א) לבחון, **בהקשר הישראלי**, כיצד ניתן למפות מערכת משולבת ומקיפה של נתיבי מים, אזורי איגום ומתקני אגירה וטיפול לנגר עילי במרקם עירוני קיים; ב) לפתח ולהדגים מתודולוגיה ליישום אמצעים לשימור נגר עילי במרחב העירוני במגמה להביא לניצול מיטבי של המים לשיפור הנוחות התרמית של הולכי רגל ברחוב ולהפחתה בצריכת האנרגיה של בניינים לאקלום.

מהלך המחקר בשנה השלישית

בניית מודל לטמפרטורת פני קרקע

אחד הגורמים בעלי השפעה רבה ביותר על מיקרו-אקלים העיר הוא טמפרטורת פני הקרקע: היא משפיעה הן על טמפרטורת האוויר בקרבתה והן על מאזן הקרינה עם עצמים ובני אדם ברחוב. לנוכחות מים בשכבות העליונות של הקרקע (בעקבות אירועי גשם) ישנה השפעה על הטמפרטורה, אשר אותה יש צורך לאמוד באמצעות מספר נתונים קטן ככל האפשר, אשר יהיה נגיש לכל מתכנן, ונתונים מטאורולוגיים סטנדרטיים בלבד. מודל כזה נבנה בפורמט המשלב אלמנטים ממספר מודלים קיימים, בהתאם לנתונים אשר צפוי כי יהיו זמינים לכל יעד בעיר. הוא נבחן בעזרת נתונים מטאורולוגיים ומדידות של פני השטח בשני אתרים בשדה בוקר, ונמצא כי הוא נותן רמות דיוק טובות. המודל תורגם לשפת מחשב FORTRAN ושולב בתוכנת CAT. המאמר המדעי

(Leaf and Erell, 2017) המציג בפירוט את המודל ומדגים את היישום שלו לחיזוי ההשפעה של צמחייה על נוחות תרמית של הולך רגל, אשר טיוטה שלו צורפה לדו"ח הקודם, הושלם והתקבל לפרסום בכתב העת Theoretical and Applied Climatology.

עדכונים למודל CAT (Canyon Air Temperature)

מודל CAT פותח מלכתחילה במטרה לספק נתוני אקלים לאתר עירוני על בסיס נתונים מדודים מתחנה מטאורולוגית אופיינית, אשר בדרך כלל ממוקמת מחוץ לעיר, למשל – בשדה התעופה (Erell & Williamson, 2006). הנתונים עשויים להיות במתכונת של שנה מטאורולוגית אופיינית, הכוללת מידע שעתי על פני שנה שלמה. בכדי לבחון את ההשפעה המצרפית על אקלים העיר של שינויים בתכסית, לרבות תוספת צמחייה, נדרשה התאמה של המודל כך שיוכל לטפל בו זמנית במספר רב של נקודות על פני כל המרחב העירוני. הקושי הראשוני בהתאמה הזאת הוא באיתור המידע הדרוש למודל ברזולוציה המרחבית המתאימה ובהזנתו למודל. לשם כך נבנה ממשק עם מערכת מידע גיאוגרפי (ממ"ג – GIS) ונתוני לווין אשר בעזרתו נרשמים מאפייני התכסית והבינוי עבור כל תא שטח. הממשק הזה נוסה בהצלחה ותואר במאמר אשר התפרסם בכתב העת Applied Geography (Kaplan et al, 2016). במהלך השנה האחרונה שוכלל מאוד הממשק הזה, על מנת שניתן יהיה לנתח את הנתונים הקיימים בממ"ג ולהזין אותם באופן שיטתי עבור מספר גדול מאוד של תאי שטח. בין היתר מתקבלים נתונים עבור אלבדו, תכסית צמחייה וגופי מים, רוחב הרחובות, הכיוון שלהם, גובה הבניינים, והחום האנתרופוגני בפרופיל המתחשב בשעות היממה ותנאי מזג האוויר.

אימות של מודל CAT המעודכן

אימות של מודל CAT המעודכן נעשה על ידי השוואה של נתונים אשר נמדדו בתחנת השירות המטאורולוגי במרכז באר שבע עם נתוני הדמיה אשר נעשו במודל CAT על בסיס נתונים מדודים מתחנה מטאורולוגית בשטח פתוח הממוקמת בסמוך ליישוב נבטים, במרחק של כ-12 ק"מ דרומית מזרחית אליה. ההבדלים בין התחנות משקפים בעיקר את השפעת מיקרו-אקלים הנוצר בעיר, אשר מתבטא בין היתר בטמפרטורות מינימום גבוהות יותר בלילות בצד טמפרטורות דומות, או אף מעט נמוכות יותר, בצהריים. ניתוח הסטטיסטי שך סימולציה אשר בוצעה עבור חודש שלם (יולי 2016) מראה כי השגיאה הממוצעת עמדה על 0.29- מעלות, עם סטיית תקן של 0.58 מעלות בלבד.

הדמיה של השונות המרחבית של טמפרטורת האוויר באמצעות מודל CAT

על מנת להדגים את יכולות מודל CAT המעודכן בהדמיה עבור עיר שלמה, בוצעה הדמיה של הטמפרטורות עבור העיר באר שבע. לשם כך חולק שטח העיר וסביבתה הקרובה ל-10,400 תאים במידות של 90X90 מטרים. הצגה גרפית של ממצאי ההדמיה בוצעה עבור תקופה של 24 שעות בימים 26-27 ביולי 2016. ההדמיה ממחישה כי תופעת אי החום העירוני אופיינית בעיקר לשעות הלילה, אם כי בשל הצפיפות הנמוכה ואופי הבינוי המפוזר העוצמה המרבית אשר נדמתה היתה כ-3 מעלות (בהשוואה לנתוני הייחוס בתחנת נבטים). בשעות היום, ובפרט בשעות הצהריים החמות, העיר אינה חמה מהשטח המדברי הפתוח המקיף אותה, ובאזורים מסוימים אף מעט קרירה יותר. מרבית כתמי הצמחייה המפוזרים בעיר הינם קטנים ובעלי השפעה מועטה על טמפרטורת האוויר. מעניין להשוות את תוצאות ההדמיה לצילומים תרמיים אשר נעשו באמצעות לווין, בשעות הבוקר (Landsat) והלילה (ASTER). בצילומים אלה ניתן להבחין בקלות בשטח הבנוי: בשעות הלילה העיר בולטת ככתם חם מוקף בקרקע לס קרירה יחסית. ביום, לעומת זאת, קרקע הלס היבשה מתחממת בקצב מהיר יותר, והעיר נראית דווקא ככתם קריר יותר מוקף בסביבה חממה יחסית. הטמפרטורה של פני השטח העירוניים אחידה למדי, ובשעות היום הנקודה החמה העיקרית בעיר היא פני השטח החשופים של בית הקברות המוסלמי הישן.

ההשפעה של צמחייה בביו-פילטר על הנוחות התרמית של הולכי רגל

מערכות הביו-פילטרים כוללות גם צמחייה אשר מיועדת לסייע בתהליך טיהור מי הנגר. לצמחייה זו עשויה להיות גם תועלת בכך שתשפר את תנאי המיקרו-אקלים בקרבתם. בין היתר נבחן שימוש בצמחים פורחים כגון אגפנתוס, עשבוניים שונים ממשפחת הכריכיים (Carex) ושיחים או עצים נמוכים ממשפחת המללויקה (Melaleuca). אף אחד מהצמחים אשר נבדקו במערכות הביו-פילטר אינו נמצא ברשימת הצמחים חסכני המים אשר פירסם משרד החקלאות, אולם ברשימה זו ישנם מינים אחרים מאותה משפחה אשר מומלץ לבדוק אם ניתן לשלב בביו-פילטרים. יחד עם זאת, חשוב להדגיש שמחקרים קודמים אשר נערכו בשדה בוקר, וכן מחקרים אחרים בארץ, הראו כי התרומה העיקרית של הצמחייה לנוחות תרמית של הולכי רגל היא בהפחתת העומס הקרינתי עליהם. בראש ובראשונה מדובר בצל המגן מקרינת שמש ישירה, אך גם לצמחי כיסוי נמוכים עשויה להיות תרומה משמעותית בכך שהם מפחיתים את שטף קרינת השמש המוחזרת ואת הקרינה האינפרא אדומה הנפלטת מפני הקרקע. תרומת הצמחייה להורדת טמפרטורת האוויר היא במקרה הטוב צנועה, ובדרך כלל אינה משמעותית. בכל מקרה, מומלץ לבחון כיצד ניתן לשלב עצים בביו-פילטרים, או לפחות בסביבתם הקרובה.

הדגמה של המתודולוגיה לבחירת אמצעים לניהול הנגר העירוני בישראל

כלי לקבלת החלטות בתכנון וניהול הנגר העירוני חייב להיות בעל המאפיינים הבאים: יכולת לחזות את כמות הנגר הנוצר ואת איכות המים בתרחישים שונים; לטפל הן בנגר העילי והן בספיקות במערכת הניקוז ובתת-הקרקע; לאפשר ביצוע ניתוחי עלות-תועלת של אמצעים שונים, בתרחישים מגוונים; ולאפשר ניתוח בקנה מרחבי מפורט מאוד, עד כדי סביבת הבית הבודד. בסקר מקיף אשר בוצע בתחילת המחקר נמצא כי הכלי היחיד אשר עומד בכל הדרישות האלה הוא תוכנה בשם SUSTAIN אשר פותח על ידי הרשות להגנת הסביבה של ממשלת ארה"ב (EPA) על בסיס מודל SWMM. הכלי הזה נבדק עבור האזור בכפר סבא אשר בו מתבצעות מדידות הנגר על ידי קבוצת מחקר אחרת בפרויקט. נמצא כי אף כי השימוש בכלי אינו פשוט ודורש מומחיות רבה, הוא מאפשר למתכנן לבחון חלופות שונות של אמצעים לניהול נגר (המכונים Best Management Practice - BMP). בדיקה נוספת של מודל ה- SUSTAIN התמקדה באופציות להתאים את ה- BMP המוצעים על ידי המודל לפתרונות ספציפיים (user-defined), כך שיתאימו הן לתנאים הסביבתיים והן לתכנון ולחומרי הבנייה המקומיים. התברר כי ניתן להגדיר פרמטרים מגוונים ואף לייצר פתרונות ספציפיים חדשים, למשל להגדיר תכונות של ביופילטר ספציפי כגון מידות, חתך קרקע מפורט, תכונות הקרקע, פרמטרים שונים של חלחול וחתכי הצנרת. בנוסף, נבדק רכיב ה- cost estimation על מנת להתאימו למחירים של חומרי הבנייה בארץ. התברר גם כי ניתן להגדיר את העלות של אלמנט שלם ולא רק עלות של רכיבי האלמנט בנפרד. בינתיים התברר כי ה- EPA האמריקאי החליט להפסיק את השדרוג והתמיכה בכלי ה- SUSTAIN, ובמקומו מוצעת גרסה מסחרית בשם InfoSWMM-SUSTAIN בעלת יכולות דומות, בעלות של כ-30 אלף דולר. כלי SUSTAIN הודגם בינתיים גם בניתוח אשר נעשה עבור העיר בת ים. הוברר שוב כי ללא מידע מפורט ברזולוציה מרחבית גבוהה, הכולל גבהים טופוגרפיים של הרחובות והמדרכות ומאפיינים של רשת הניקוז התת-קרקעית, לא ניתן להפיק מהכלי את המירב.